NUREG/IA-0548

International Agreement Report

Assessment of TRACE V5.0 Patch 7 Using OECD-ATLAS2 B3.2 Test

Prepared by:
Seung Hun Yoo*, Kyung-Won Lee*, Dong Gu Kang*, Andong Shin*

*Korea Institute of Nuclear Safety (KINS)
62 Gwahak-ro, Yuseong-gu,
Daejeon 34142, Republic of Korea

K.Tien, NRC Project Manager

Division of Systems Analysis
Office of Nuclear Regulatory Research
U.S. Nuclear Regulatory Commission
Washington, DC 20555-0001

Manuscript Completed: February 2024
Date Published: April 2024

Prepared as part of
The Agreement on Research Participation and Technical Exchange
Under the Thermal-Hydraulic Code Applications and Maintenance Program (CAMP)

Published by
U.S. Nuclear Regulatory Commission

AVAILABILITY OF REFERENCE MATERIALS IN NRC PUBLICATIONS

NRC Reference Material

As of November 1999, you may electronically access NUREG-series publications and other NRC records at NRC's Library at www.nrc.gov/reading-rm.html. Publicly released records include, to name a few, NUREG-series publications; *Federal Register* notices; applicant, licensee, and vendor documents and correspondence; NRC correspondence and internal memoranda; bulletins and information notices; inspection and investigative reports; licensee event reports; and Commission papers and their attachments.

NRC publications in the NUREG series, NRC regulations, and Title 10, "Energy," in the *Code of Federal Regulations* may also be purchased from one of these two sources.

1. **The Superintendent of Documents**
   U.S. Government Publishing Office
   Washington, DC 20402-0001
   Internet: https://bookstore.gpo.gov/
   Telephone: (202) 512-1800
   Fax: (202) 512-2104

2. **The National Technical Information Service**
   5301 Shawnee Road
   Alexandria, VA 22312-0002
   Internet: https://www.ntis.gov/
   1-800-553-6847 or, locally, (703) 605-6000

A single copy of each NRC draft report for comment is available free, to the extent of supply, upon written request as follows:

Address: **U.S. Nuclear Regulatory Commission**
Office of Administration
Digital Communications and Administrative Services Branch
Washington, DC 20555-0001
E-mail: Reproduction.Resource@nrc.gov
Facsimile: (301) 415-2289

Some publications in the NUREG series that are posted at NRC's Web site address www.nrc.gov/reading-rm/doc-collections/nuregs are updated periodically and may differ from the last printed version. Although references to material found on a Web site bear the date the material was accessed, the material available on the date cited may subsequently be removed from the site.

Non-NRC Reference Material

Documents available from public and special technical libraries include all open literature items, such as books, journal articles, transactions, *Federal Register* notices, Federal and State legislation, and congressional reports. Such documents as theses, dissertations, foreign reports and translations, and non-NRC conference proceedings may be purchased from their sponsoring organization.

Copies of industry codes and standards used in a substantive manner in the NRC regulatory process are maintained at—

The NRC Technical Library
Two White Flint North
11545 Rockville Pike
Rockville, MD 20852-2738

These standards are available in the library for reference use by the public. Codes and standards are usually copyrighted and may be purchased from the originating organization or, if they are American National Standards, from—

American National Standards Institute
11 West 42nd Street
New York, NY 10036-8002
Internet: www.ansi.org
(212) 642-4900

Legally binding regulatory requirements are stated only in laws; NRC regulations; licenses, including technical specifications; or orders, not in NUREG-series publications. The views expressed in contractor prepared publications in this series are not necessarily those of the NRC.

The NUREG series comprises (1) technical and adminis-trative reports and books prepared by the staff (NUREG–XXXX) or agency contractors (NUREG/CR–XXXX), (2) proceedings of conferences (NUREG/CP–XXXX), (3) reports resulting from international agreements (NUREG/IA–XXXX),(4) brochures (NUREG/BR–XXXX), and (5) compilations of legal decisions and orders of the Commission and Atomic and Safety Licensing Boards and of Directors' decisions under Section 2.206 of NRC's regulations (NUREG–0750),and (6) Knowledge Management prepared by NRC staff or agency contractors.

NUREG/IA-0548

International Agreement Report

Assessment of TRACE V5.0 Patch 7 Using OECD-ATLAS2 B3.2 Test

Prepared by:
Seung Hun Yoo*, Kyung-Won Lee*, Dong Gu Kang*, Andong Shin*

*Korea Institute of Nuclear Safety (KINS)
62 Gwahak-ro, Yuseong-gu,
Daejeon 34142, Republic of Korea

K. Tien, Project Manager

Division of Systems Analysis
Office of Nuclear Regulatory Research
U.S. Nuclear Regulatory Commission
Washington, DC 20555-0001

Manuscript Completed: February 2024
Date Published: April 2024

Prepared as part of
The Agreement on Research Participation and Technical Exchange
Under the Thermal-Hydraulic Code Applications and Maintenance Program (CAMP)

Published by
U.S. Nuclear Regulatory Commission

ABSTRACT

The assessment of TRACE V5.0 Patch 7 was performed using the OECD-ATLAS2 B3.2 test which is a 100% Direct Vessel Injection line break in the ATLAS referring to the APR1400. TRACE showed a generally good agreement with most of the sequence of events of the experiment including the injection timing of the Emergency Core Cooling System (ECCS), the minimum core level, and the occurrence of Loop Seal Clearing (LSC) but delayed in the core quenching time. The predicted integrated discharge flow, the mass flow rate of cold legs and hot legs, and the ECCS flow were well-matched with the experiment. TRACE predicted the same Maximum Cladding Temperature (MCT) at the same timing as the experiment. However, the predicted position of the MCT was different from the experiment due to the different predicted local behaviors and the predicted core quenching time was delayed. Through sensitivity studies, it was found that the cladding temperature generally increased in proportion to the break size and the most decisive factor in determining the cladding temperature is the behavior of the minimum core level. In conclusion, TRACE showed an excellent capability to predict the same MCT at the same timing as the experiment. However, it showed a reasonable capability to predict the pressure drop in the reactor vessel for the region of the steam-dominant two-phase flow, the recovery of the core level, and the core quenching time.

FOREWORD

This report represents one of the in-kind contributions submitted to fulfill the bilateral agreement for cooperation in thermal-hydraulic activities between the Korea Institute of Nuclear Safety (KINS) and the U.S. Nuclear Regulatory Commission (NRC) in the form of a Korean contribution to the NRC's Code Assessment and Maintenance Program (CAMP), the main purpose of which is to validate the TRACE code.

Since 2006, the integral effect test facility, Advanced Thermal-Hydraulic Test Loop for Accident Simulation (ATLAS) has been operated by the Korea Atomic Energy Research Institute (KAERI), which was constructed to simulate the behavior of the reactor coolant system during transients in its reference designs, Advanced Power Reactor 1400 MWe (APR1400). After a series of the Direct Vessel Injection (DVI) line break tests in the ATLAS was completed for four break sizes, 5%, 25%, 50%, and 100%, KAERI proposed the OECD-ATLAS project as an international joint project. The OECD-ATLAS2 B3.2 test was carried out during the OECD-ATLAS phase 2, aiming at assessing the capability of the thermal-hydraulic codes for an Intermediate Break Loss of Coolant Accident (IBLOCA), which simulates a 100% DVI line break in the APR1400.

This report describes the TRACE code assessment for an IBLOCA in the ATLAS facility which simulates a 100% DVI line break in the APR1400. According to the CAMP program and the OECD-ATLAS2 project, this report has been reviewed by NRC, KINS, KAERI, and the members of the OECD-ATALS2 project.

TABLE OF CONTENTS

LIST OF FIGURES

LIST OF TABLES

EXECUTIVE SUMMARY

An integral effect test on the Intermediate Break Loss of Coolant Accident (IBLOCA) of the ATLAS facility which has an equivalent size of 100% Direct Vessel Injection (DVI) line break of the APR1400 was conducted according to the OECD/NEA's ATLAS2 project. As the nuclear industry is trying to exclude the Large Break Loss of Coolant Accident (LBLOCA) from the design of the advanced nuclear reactor or the small modular reactor, the deep understanding and the importance of the code predictive capability of the IBLOCA are likely to be increased in the future. This study aims at assessing the predictive capability of TRACE V5.0 Patch 7 against the OECD-ATLAS2 B3.2 Test, which is an IBLOCA and simulates a 100% DVI line break of the APR1400.

Regarding the TRACE input model, the Reactor Pressure Vessel (RPV) was modeled by a VESSEL component consisting of twenty axial levels, six azimuthal sectors, and four radial rings. The Steam Generators (SGs) with U-tubes, the Hot Legs (HLs), the Cold Legs (CLs), the PZR (Pressurizer), and connecting piping were modeled by a combination of one-dimensional PIPE components. The Emergency Core Cooling System (ECCS) including the Safety Injection Pump (SIP) and the Safety Injection Tank (SIT) with appropriate control logics, a total of 124 heat structures, and four POWER components were also modeled. To properly simulate the behavior of the Loop Seal Clearing (LSC), the Counter Current Flow Limitation (CCFL) model was applied to a total of 4 regions: the Fuel Alignment Plate, Hot Leg Riser, Inlet of SG U-tubes, and Outlet of Intermediate Legs. The discharge coefficients of the Ransom-Trapp model were optimized for the break at the DVI line and the Main Steam Safety Valves.

Through the null transient calculation of TRACE, the results of steady-state calculation were analyzed and compared to the maximum of the measurement uncertainty and the acceptance criteria presented in the TRACE Modeling Guidance. All parameters reached the steady-state condition and were satisfied with the either of the two criteria.

TRACE showed a generally good agreement with most of the sequence of events of the experiment including the opening and closing time of the MSSVs, the injection timing of the SIP and SIT, the minimum core level, and the occurrence of the LSC. However, it predicted a delayed core quenching time after the LSC. It was confirmed that the calculated total core power was the same as the experiment, including the decay curve. The predicted integrated mass of discharge flow and the mass flow rate of the SIP, SITs, CLs, and HLs were well-matched with the experiment. Although the predicted pressure drop in the RPV presented a good agreement with the experiment for the region of the liquid-dominant two-phase flow, it indicated a more rapid pressure drop than the experiment for the region of the steam-dominant two-phase flow. TRACE predicted the same Maximum Cladding Temperature (MCT) at the same timing as the experiment. However, the predicted position of the MCT in the heater group was different from the experiment because the local behavior predicted by the calculation was different from the experiment. Due to the delayed core level recovery and the LSC, the predicted core quenching time was delayed.

Sensitivity studies were carried out for the different break sizes and positions. As a result of the sensitivity studies for the break sizes, it was found that the cladding temperature generally increased in proportion to the break size under the condition of the same break size. Through the sensitivity studies for the break positions, it was found that there could be a vulnerable break position due to the randomness of the LSC, which may show a higher cladding temperature although the break size is the same. It was also found that the most decisive factor in

determining the cladding temperature is the behavior of the minimum core level resulting from the complex behavior of the LSC and the upper downcomer rather than whether or not the additional SIP was activated.

In conclusion, TRACE showed a good agreement with the experiment for the most sequence of events and transient behaviors in the major parameters. TRACE showed an excellent capability to predict the same MCT at the same timing as the experiment. However, it showed a reasonable capability to predict the pressure drop in RPV for the region of the steam-dominant two-phase flow, the recovery of the core level, and the core quenching time.

ABBREVIATIONS AND ACRONYMS

APR1400	Advanced Power Reactor 1400 MWe
ATLAS	Advanced Thermal-Hydraulic Test Loop for Accident Simulation
BETHSY	Boucle d`Etudes Thermohydrouliques Systeme
CAMP	Code Application and Maintenance Program
CCFL	Counter Current Flow Limitation
CL	Cold Leg
DEGB	Double-Ended Guillotine Break
DVI	Direct Vessel Injection
ECCS	Emergency Core Cooling System
FLB	Feedwater Line Break
HL	Hot Leg
IBLOCA	Intermediate Break Loss of Coolant Accident
IET	Integral Effect Test
KAERI	Korea Atomic Energy Research Institue
KINS	Korea Institute of Nuclear Safety
LBLOCA	Large Break Loss of Coolant Accident
LOBI	LWR Off-normal Behaviour Investigations
LOCA	Loss of Coolant Accident
LOFT	Loss of Fluid Test
LPP	Low Pressurizer Pressure
LSC	Loop Seal Clearing
LSTF	Large Scale Test Facility
MCT	Maximum Cladding Temperature
MFIV	Main Feedwater Isolation Valve
MLOCA	Medium Loss of Coolant Accident
MSIV	Main Steam Isolation Valve
MSLB	Main Steam Line Break
MSSV	Main Steam Safety Valve
NEA	Nuclear Energy Agency
NRC	Nuclear Regulatory Commission
OECD	Organization for Economic Co-operation and Development
PCT	Peak Cladding Temperature
PMK-2	Paks Model Circuit-2 (in Hungarian)

PZR	Pressurizer
RCP	Reactor Coolant Pump
RCS	Reactor Coolant System
RPV	Reactor Pressure Vessel
SBLOCA	Small Break Loss of Coolant Accident
SG	Steam Generator
SGTR	Steam Generator Tube Rupture
SIP	Safety Injection Pump
SIT	Safety Injection Tank

1 INTRODUCTION

U.S. Nuclear Regulatory Commission (NRC) takes a risk-informed regulation and maintains a set of risk models for the operating commercial nuclear power plant in the United States. According to the documentation on the estimated Loss of Coolant Accident (LOCA) frequencies [1], the rates of initiating events [2,3], and the assessment of accident risks for US nuclear power plants [4], the break size of the Intermediate Break Loss of Coolant Accident (IBLOCA) in the pressurized water reactor can be regarded from 2.0 to 6.0 inches or from 1.625 to 7.0 inches. The different estimations of the break size for the IBLOCA generally originated from the different expert elicitation processes or the use of different types of aggregation techniques [5]. Moreover, the break size of the IBLOCA also can be influenced by the design and the power of the nuclear power plant. Then IBLOCA or Medium LOCA (MLOCA) can be defined as considering the following functional aspect, which could be more generally accepted and classified regardless of the plant characteristics.

“The medium LOCA initiating event is defined as a steam or liquid break that is large enough to remove decay heat without using the steam generators but small enough that RCS pressure is above the safety injection tanks and low-pressure injection system shutoff pressure [5].”

From a regulatory perspective, the IBLOCA has not been addressed in the Final Safety Analysis Report of the nuclear power plant and received less attention than the Large Break LOCA (LBLOCA) or Small Break LOCA (SBLOCA). However, as the nuclear industry is trying to exclude the LBLOCA from the design of the advanced nuclear reactor or the small modular reactor, the deep understanding and the importance of IBLOCA are likely to be increased in the future from the viewpoint of the safety evaluation in the nuclear power plant.

On the other hand, on the research side, experiments for diverse IBLOCA scenarios were carried out. Table 1-1 shows the summary of the IBLOCA experiments in the different facilities [6]. There were the IBLOCA experiments in the facilities of LSTF, LOBI, LOFT, BETHY, PMK-2, and ATLAS simulating the break in the Cold Leg (CL), the Hot Leg (HL), the Pressurizer (PZR) surgeline, the Emergency Core Cooling System (ECCS) nozzle, and the Direct Vessel Injection (DVI) line. Those tests mostly showed the occurrence of the Peak Cladding Temperature (PCT). Among the tests, the ATLAS2 B3.2 test was selected to benchmark the TRACE code. This test was carried out during the OECD/NEA-ATLAS phase 2 project, which operated from 2017 to 2020. It is classified as an IBLOCA scenario simulating the Advanced Power Reactor 1400 MWe (APR1400) nuclear power plant.

Adequacy criteria are applied for assessing the code calculations. The criteria have four levels of agreement: excellent, reasonable, minimal, and insufficient. The criteria are assigned based on comparisons of the magnitudes and trends of the calculated and measured data in the context of the uncertainty in the experimental data. Judgments showing excellent or reasonable agreement are considered acceptable, while minimal agreement is considered conditionally acceptable and insufficient agreement is considered unacceptable. Analyses performed using the computer code must appropriately account for the large uncertainties associated with code models for which minimal or insufficient judgments have been made [7].

Table 1-1 Summary of IBLOCA Experiments

Test Facility	Volume Scale	Break Position	Break Size	Occurrence of PCT
LSTF	1/48	Surgeline ECCS nozzle	17% CL 13% CL	O O
LOBI	1/712	CL HL	10% to 25% CL 25% HL	- -
LOFT	1/60	ECCS nozzle	14% CL	O
BETHSY	1/100	CL	5% CL	O
PMK-2	1/2070	Surgeline	DEGB	O
ATLAS (A4.1)	1/288	ECCS nozzle	17% CL	O
ATLAS (A5.2)	1/288	ECCS nozzle	13% CL	O
ATLAS2 (B3.1)	1/288	Surgeline	-	-
ATLAS2 (B3.2)	1/288	DVI line	100% DVI (8% CL)	O

2 DESCRIPTION OF ATLAS FACILITY

Advanced Thermal-hydraulic Test Loop for Accident Simulation (ATLAS) is an Integral Effect Test (IET) facility that can simulate various accidents and transient phenomena of the APR1400 nuclear power plant has been designed and operated by KAERI (Korea Atomic Energy Research Institute) [8]. The APR1400, which is the prototype of the ATLAS, has a thermal power of 4000 MW and a loop configuration of two HLs and four CLs for the Reactor Coolant System (RCS) [8].

The ATLAS facility has the same loop configuration as the APR1400 but was scaled down according to Ishii and Kataoka's three-level scaling law [9]. The ATLAS has a half-height and 1/288-volume scale test facility to the APR1400 [8]. It is known that the motivation for adopting the reduced-height design is to investigate an integrated annular downcomer where multi-dimensional phenomena may occur under the injection of the emergency core cooling water through the DVI line [10]. Since the ATLAS facility is half the height of the prototype, the time of the ATLAS is $\sqrt{2}$ times faster than the prototype time. However, the ATLAS preserved the pressure, the temperature rise in the core and steam, the gravity, the subcooling, and the hydraulic diameter as the unity [10]. The ATLAS was also designed to give precise flow resistance to maintain the pressure drop ratio of the half.

Figure 2-1 shows a schematic diagram of a loop connection of ATLAS [11]. The ATLAS consists of a primary system, a secondary system, a safety injection system, a break simulating system, a containment simulating system, and auxiliary systems as shown in Figure 2-2 [11]. The primary system includes one Reactor Pressure Vessel (RPV), two HLs, four CLs, a PZR, four Reactor Coolant Pumps (RCPs), and two Steam Generators (SGs). The safety injection system consists of four Safety Injection Tanks (SITs), a Safety Injection Pump (SIP) simulating 400% safety injection and long-term cooling, a charging pump for auxiliary spray, and a shutdown cooling pump for low pressure safety injection and shutdown cooling operation. The secondary system of the ATLAS is simplified to be a circulating loop-type. The steam generated at SGs is condensed in a direct condenser tank and the condensed feedwater is again injected into the SGs. The break simulation system consists of several break simulating lines such as LBLOCA, DVI line break LOCA, SBLOCA, Steam Generator Tube Rupture (SGTR), Main Steam Line Break (MSLB), and Feedwater Line Break (FLB) [8, 11].

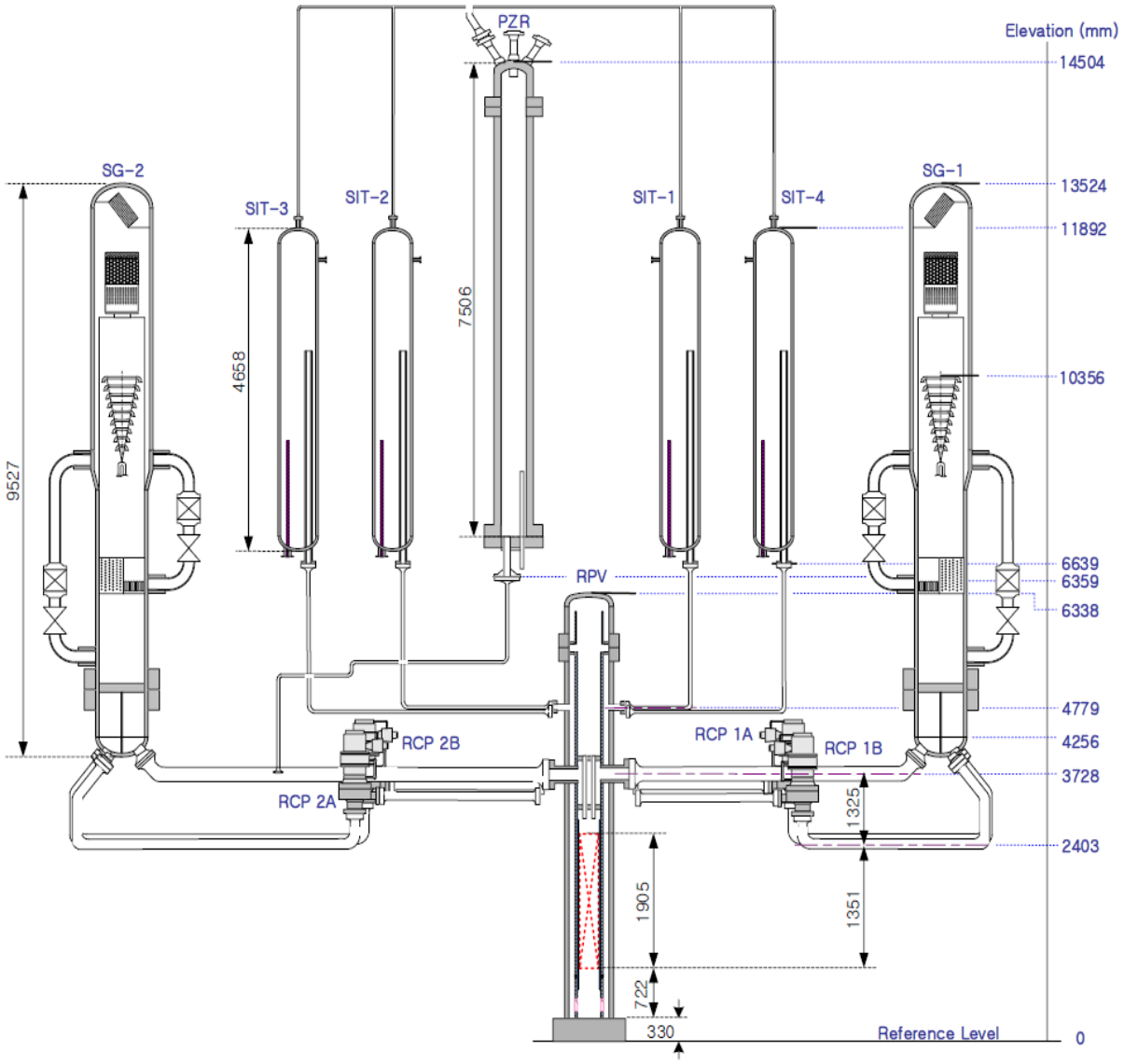

Figure 2-1 Schematic Diagram of Loop Connection of ATLAS

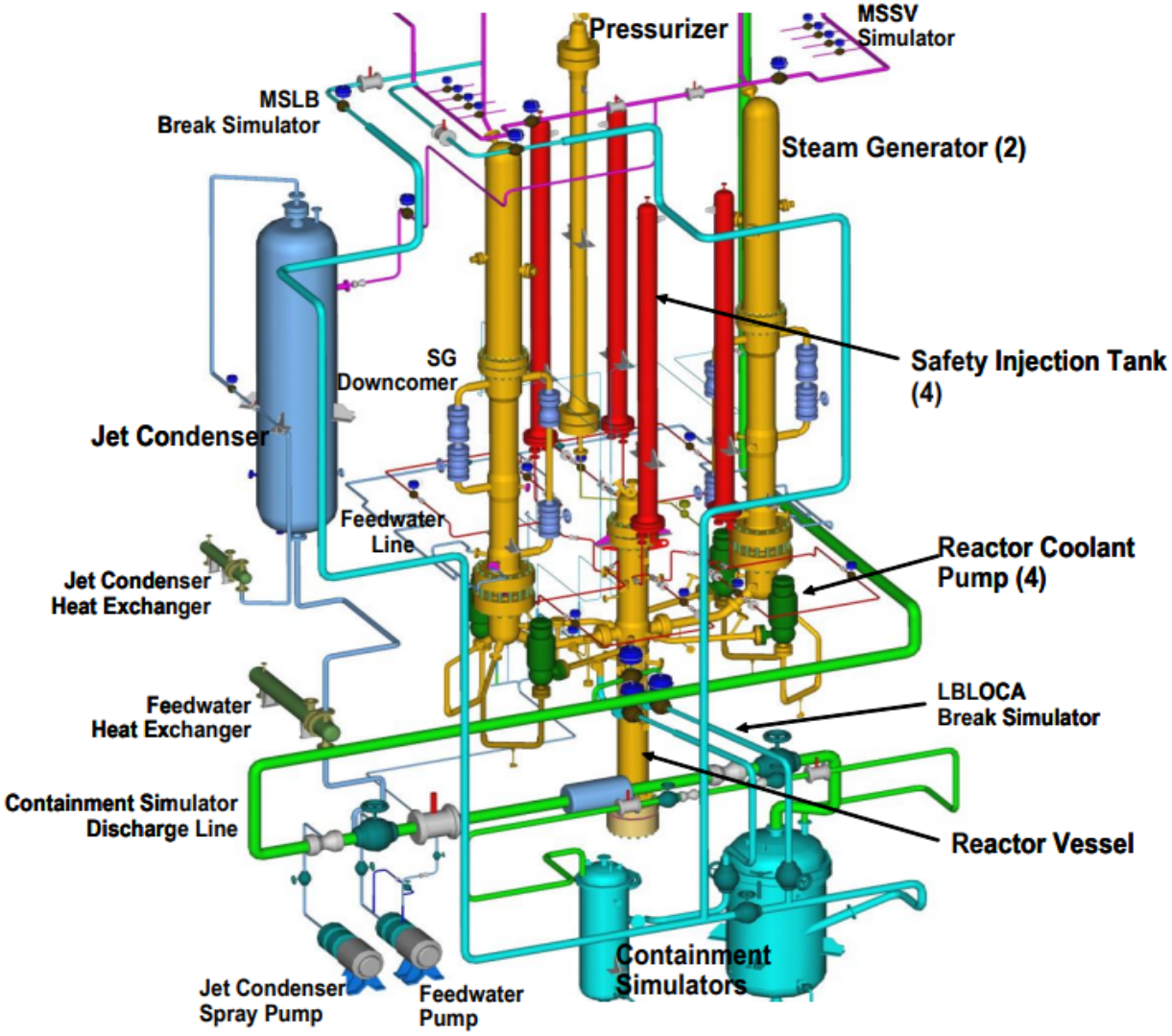

Figure 2-2 Three-Dimensional View of ATLAS

3 DESCRIPTION OF THE OECD-ATLAS2 B3.2 TEST

The OECD-ATLAS2 project is a follow-up phase to the first phase of the OECD ATLAS Joint project, which operated from 2014 to 2017. The OECD-ATALS2 project started in October 2017 for three years. Due to the worldwide crisis resulting from the COVID-19 pandemic, the project was extended until the end of 2020 [11]. According to the agreement of the OECD-ATLAS2 project, the experimental results will not be opened until the end of 2023. Therefore, all experimental results in this report will be presented in the non-dimensional form.

A total of 8 tests were performed in phase 2 including passive core makeup during station blackout, SBLOCA, IBLOCA, SLB followed by SGTR, and shutdown coolability without residual heat removal system. Among the tests, the B3.2 test was the simulation of the 100% DVI line break, which corresponds to an 8.5-inch break in the APR1400. Although the B3.2 test had a smaller break size than the B3.1 test, which is the simulation of the PZR surgeline break, the B3.2 test caused an increase in the steam pressure in the core and an excursion behavior of the cladding temperature compared with the B3.1 test [12].

The initial steady-state conditions in the B3.2 test were determined based on those of the APR1400 and by applying the scaling ratio of each parameter. Due to a limitation of core power simulation in the ATLAS facility, the steady-state condition was achieved at about 8% of ideally scaled core power considering a heat loss compensation. The decay heat in the core of the ATLAS was simulated by 1.2 times the ANS-73 decay curve from a conservative point of view. In the B3.2 test, a uniform radial power distribution was applied, so that all heater rods in the core had an equivalent thermal power. For axial power distribution, a chopped cosine power curve was applied [8].

Figure 3-1 indicates an overall configuration of the safety injection and break location of the B3.2 test [8]. It was assumed that the 100% DVI line break occurred at the DVI line 3. The break area of the DVI line 3 corresponds to the 8.5-inch break and 8% of the CL flow area in the APR1400. The safety injection water was only injected through the intact DVI nozzles, which are the DVI line 1, 2, and 4. It was also assumed that there was off-site power simultaneously with a loss of a diesel generator, which is regarded as the worst single failure, causing the minimum injection flow of the emergency core cooling water. Then, the SIT-1, 2, and 4 were credited and the SIT-3 was not credited due to the assumption of the Double-Ended Guillotine Break (DEGB) of the DVI line 3. The upper region of the SIT was filled with nitrogen gas of 4.3 MPa. The actuation of the fluidic device inside the SIT in the APR1400 was simply simulated by the simulation of the valve opening and closing on the SIT line in the ATALS. When the level of the SIT in the ATLAS reached 2.0 m, the valve on the SIT was closed to terminate the injection of the SIT flow, so that the possibility of nitrogen inflow to the RCS was excluded during the test [13]. The SIP-1 was only operated and the SIP-2 and 4 were excluded due to the single failure assumption of a failure of a diesel generator [8].

Figure 3-2 presents the isometric drawing of the break flow piping [8]. In the break flow piping, there is a break nozzle to simulate the break geometry and area, a quick open valve to initiate the accident, and a condensation tank to accumulate the discharged RCS inventory and the emergency core cooling water. The condensation tank was maintained as the atmospheric pressure to simulate the containment of the APR1400 [8].

When the ATLAS facility reached the specified initial conditions, the balance between the primary and the secondary systems were maintained for more than 30 minutes. After storing the

data during this steady-state period, the test was initiated by opening the quick open valve (OV-BS-11) in Figure 3-2. The scaled down set-point and delay time for the trip signal of major components in the B3.2 test were as follows [8].

- Low pressurizer pressure (LPP) signal: Pressurizer pressure < 10.72 MPa
- Reactor trip: Coincident with LPP signal
- Main steam isolation valve (MSIV) close: X seconds delay after the LPP signal
- Main feedwater isolation valve (MFIV) close: X seconds delay after the LPP signal
- SIP initiation: XX seconds delay after the LPP signal
- SIT initiation: Downcomer pressure < 4.03 MPa

Discharge of the secondary system inventory was available through the Main Steam Safety Valves (MSSVs). The MSSV was designed to be opened at 8.1 MPa and closed at 7.7 MPa, depending on the secondary system pressure of each SG. The auxiliary feedwater to the secondary system was not supplied during the whole transient of the B3.2 test [8].

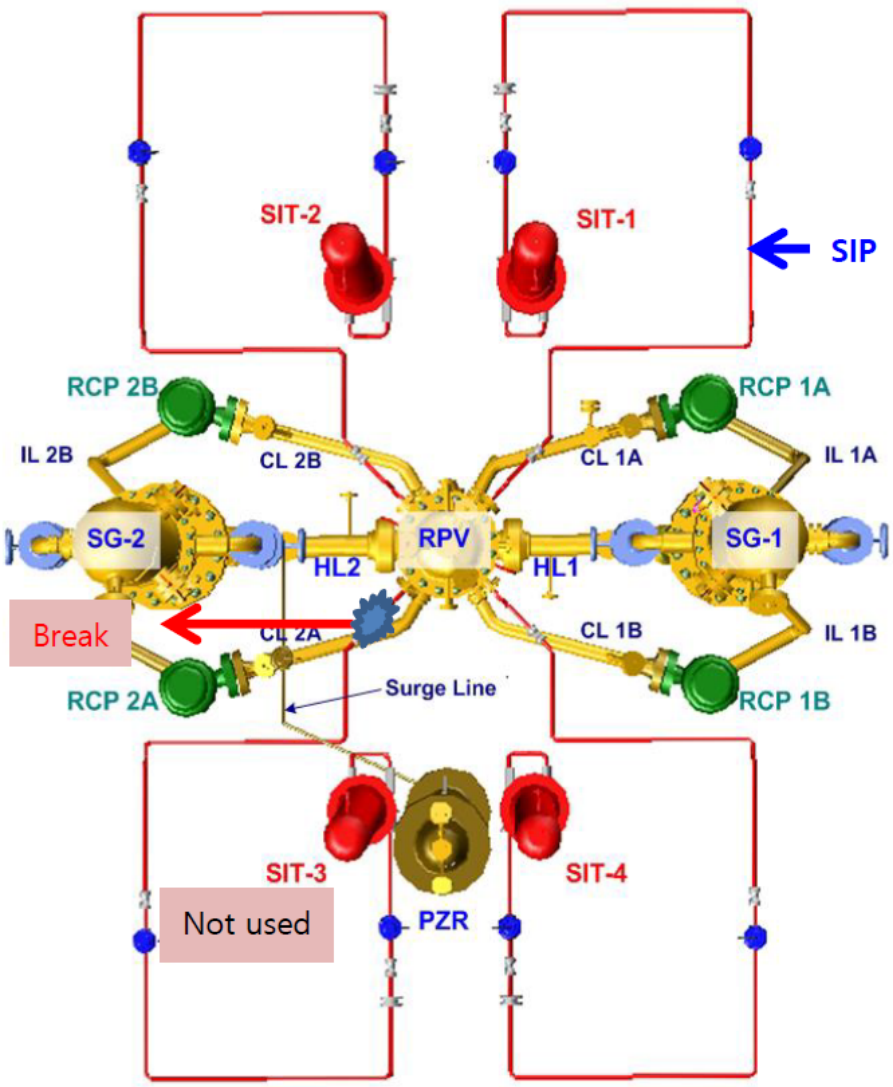

Figure 3-1 Location of the Break Unit and SI System

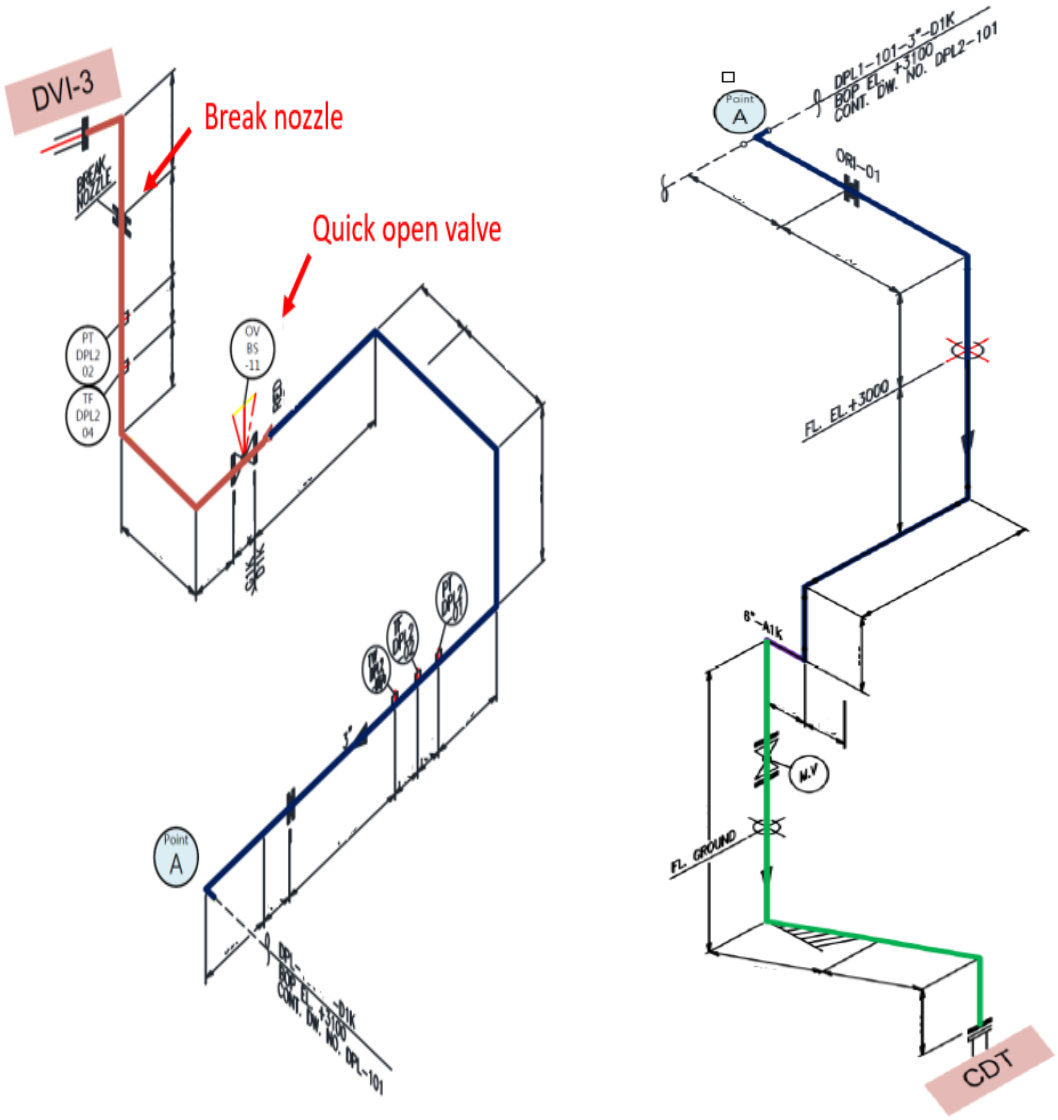

Figure 3-2 Isometric Drawing of the Break Flow Piping

4 DESCRIPTION OF TRACE INPUT MODELS

TRACE has been developed to perform best-estimate analysis of LOCA, operational transient, and other accident scenarios in the nuclear power plant. TRACE takes a component-based approach to modeling a reactor system. Each physical piece of equipment in a flow loop can be represented as some type of component, and each component can be further nodalized into some number of physical volumes (also called cells) over which the fluid, conduction, and kinetics equations are averaged [14]. The TRACE input model for the OECD-ATLAS2 B3.2 test was developed based on the KINS TRACE model for the assessment of condensation models using PASCAL tests, which was suggested by Lee et al. [15].

Figure 4-1 presents the schematic nodalization of TRACE for the ATLAS2 B3.2 test. In this study, the RPV was modeled with a VESSEL component which enables to simulate the multi-dimensional flow distribution, the emergency core cooling bypass, and upper plenum pool formation. The primary and secondary sides of the steam generator with U-tubes, the HLs, the CLs, the pressurizer, and connecting piping are made of a combination of one-dimensional PIPE components. The Reactor Coolant Pumps (RCPs) and the valves for the secondary system such as MSSVs were modeled considering those experimental results and characteristics over the pressure, respectively. To reflect the heat structure characteristics of each hydraulic component, a total of 124 heat structures were created by appropriately dividing the region of each hydraulic component and allocating corresponding heat structures. A total of 4 power components were modeled to simulate one hot rod and three separate power groups from the core to the downcomer. Using the FILL components, the SIP in the safety injection system and the main feedwater, and the auxiliary feedwater of the SGs were modeled and treated as the boundary conditions. The control logics for the accident initiation, the sequential actuation of the safety-related components and the MSSVs, the calculation of the collapsed water levels in the major components, and the heat loss simulation were modeled by the control blocks. The following describes the major components and models of the B3.2 test.

4.1 Reactor Pressure Vessel

The RPV was modeled by a VESSEL component. The axial level of the core consisted of a total of 20 cells which includes 11 cells for the active core from the second level to the thirteenth level (z2 ~ z13) [16]. The number of axial levels was determined considering the core power distribution and the TRACE PWR Modeling Guidance [17]. Figures 4-2 and 4-3 show the radial rings and the azimuthal sectors of the core, respectively [16]. The radial direction of the core was divided into 4 regions including 3 regions for fuel assemblies and 1 region for the downcomer [16].

The reason for configuring 3 radial rings in the fuel region is that the ATLAS test was carried out with 3 heater groups in the fuel region. And it is to properly set the Reflood option in the TRACE because a heat structure to which Reflood is applied must be connected to each cell in the radial and circumferential directions of the vessel. The outermost ring which is the ring number 4 represents the downcomer region. It is divided into a total of 6 azimuthal sectors at an angle of 60 degrees in the azimuthal direction, considering the overall configuration of the HLs, the CLs, and the DVI lines. The CL 1B is started as the sector 1, and the nodes were configured so that the azimuthal sector number increases by one in the counterclockwise direction [16].

4.2 Pressurizer

The surgeline of the PZR was modeled reflecting the iso-drawing of the surgeline piping in the experiment. A total of 9 cells were applied to simulate the PZR. A valve and a BREAK component were connected to the top of the PZR for the primary pressure control under the steady-state calculation. A FILL component was also connected to the bottom of the PZR to control the level of the PZR at the steady-state condition. The surgeline PIPE component was connected to the PZR PIPE component using the Offtake model of 90 degrees [16].

4.3 Steam Generator

The U-tube of each SG was modeled by a PIPE component having the average height of the real experimental component and a total of 18 cells. The upper bended region consisted of 4 cells to form a semicircle based on the experimental inner diameter of the U-Bend. The secondary side of the SG was modeled by dividing the region into the dry dome, the separator, the evaporator, the economizer, and the annular downcomer. Considering the main flow direction, the connection between each PIPE component was connected by the axial flow junction. It was assumed that the separator discharged pure steam to the dry dome using the ideal separator model.

4.4 Intermediate Leg and Counter Current Flow Limitation Model

Figure 4-4 indicates the nodalization of the intermediate legs. The axial region connected to the reactor vessel and that connected to the SG were defined as the upflow and the downflow, respectively. The intermediate legs consist of 11 cells. The modeling of the intermediate legs is important because it is intimately related to the simulation of the Counter Current Flow Limitation (CCFL). And the behavior of the CCFL is directly related to the prediction of the core water level and the PCT. The conventional model of the intermediate leg was improved by the sensitivity studies and the reflection of the NRC's research that changed the nodalization of the 90 degrees elbow, which divided the 90 degrees elbow from 1 cell to 2 cells [16].

According to appendix A.26 of the TRACE PWR Modeling Guidance [17], the guidance addressed the importance of the appropriate modeling of the CCFL and provided a set of the recommended CCFL inputs validated by such as the LOFT, BETHSY, and Semiscale experiments. In this study, the CCFL model was applied to a total of 4 regions as follows.

- Fuel Alignment Plate in the Reactor Vessel: 1 Position
- Hot Leg Riser: 2 Positions
- Inlet of SG U-tubes: 2 Positions
- Outlet of Intermediate Legs: 4 Positions

4.5 Break Piping System

As shown in Figure 4-5, the break piping system was modeled and consisted of a break nozzle, piping, a quick open valve, and a condensation tank. In this system, the break nozzle was modeled to reflect the break area and hydraulic diameter of the experiment, and the Ransom-Trapp model was applied to the edge of the break nozzle as a choked flow model. The piping was modeled by simplifying the entire shape of the experiment while maintaining the loss

coefficient of elbows and the elevation change of the piping in the experiment. The quick open valve was modeled considering the minimum flow area of the valve design. The condensation tank simulated the containment of a real power plant, and the pressure of the condensation tank over time measured in the experiment was observed to be almost constant, so it was modeled as a constant pressure during the transient.

4.6 Main Steam Safety Valve

Three MSSVs of ATLAS are installed in the steam line of each SG, but only one MSSV was opened in the B3.2 test. The number 1 of the MSSV valve receives the dry dome pressure of each SG as an input and is modeled to open when it exceeds 8.1 MPa and close when it falls below 7.7 MPa. The specific modeling of the maximum valve rate of each MSSV was improved and validated with the OECD-ATLAS A1.2 test in the modeling optimization process of the previous study [16]. The Ransom-Trapp model was applied to each MSSV to simulate the choked flow.

4.7 Ransom-Trapp Model

The choked flow occurs when the mass flow in a pipe becomes independent of the downstream conditions. TRACE provides the Ransom-Trapp model for the simulation of the choked flow [18]. In this study, the Ransom-Trapp model was applied to the edge of the break nozzle and the number 1 valves of MSSVs as the following optimized user-defined subcooled and two-phase multipliers. The multipliers were determined by sensitivity studies that varied the combination of two multipliers in different two positions.

- Break Nozzle: C_{sub}=0.94, C_{tp}=0.91
- MSSVs: C_{sub}=1, C_{tp}=1

4.8 Heat Loss

Heat loss was applied only to the outer wall of the RPV on the primary side and the water region of the steam generator on the secondary side. Therefore, HLs, CLs, intermediate legs, PZR, surgeline, and the steam piping on the secondary side, etc. were assumed to be adiabatic. The heat loss of each heat structure was calculated using a heat transfer coefficient table according to the average surface temperature. This heat transfer coefficient simulates the natural convective cooling that occurs through the outer wall of the ATLAS facility. The initial table of the heat transfer coefficient consisted of the values confirmed by the validation of the ATLAS experiment simulating the heat loss effect. Then, these original values were modified iteratively to satisfy the total heat loss observed in the experiment of the B3.2 test.

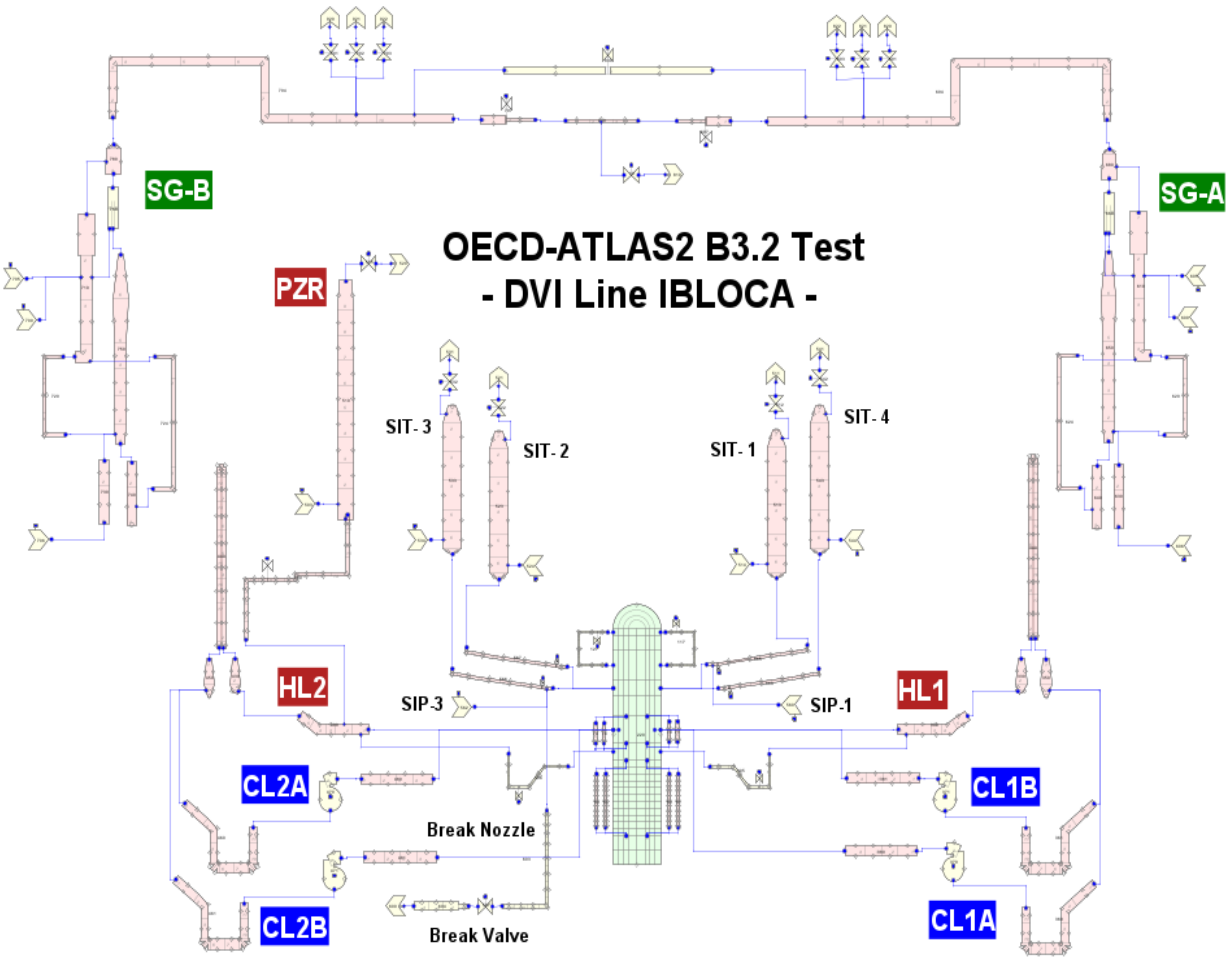

Figure 4-1 Schematic Nodalization of TRACE for ATLAS2 B3.2 Test

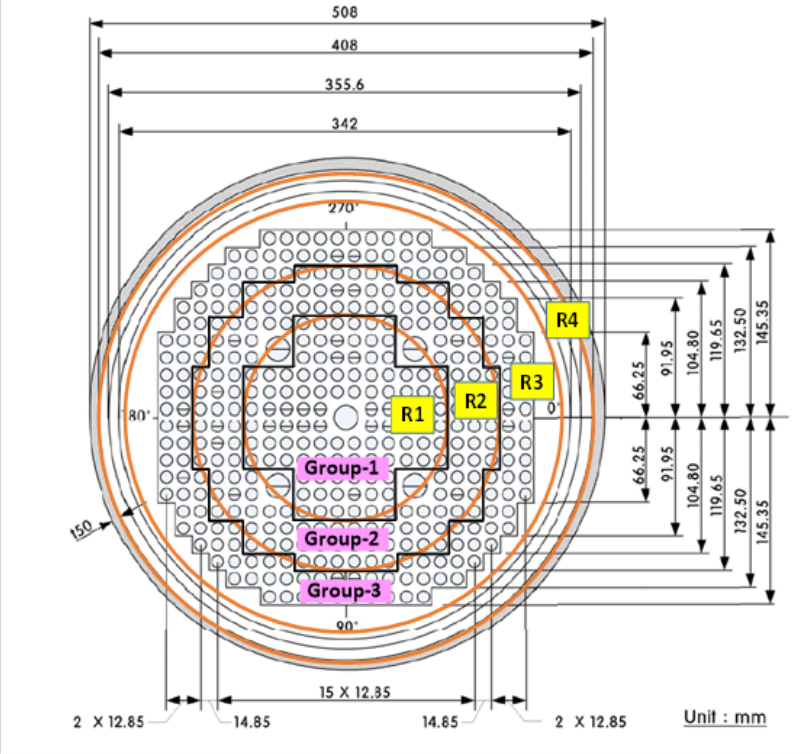

Figure 4-2 Radial Rings of the Core

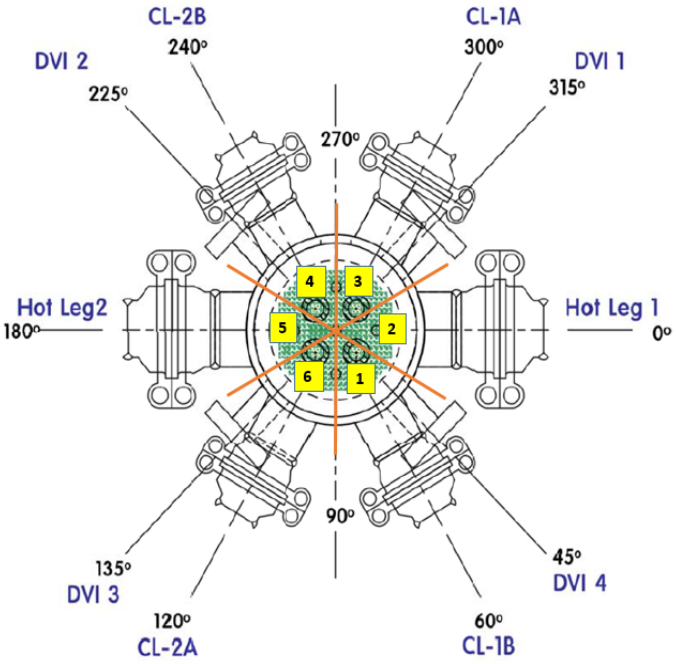

Figure 4-3 Azimuthal Sectors of the Core

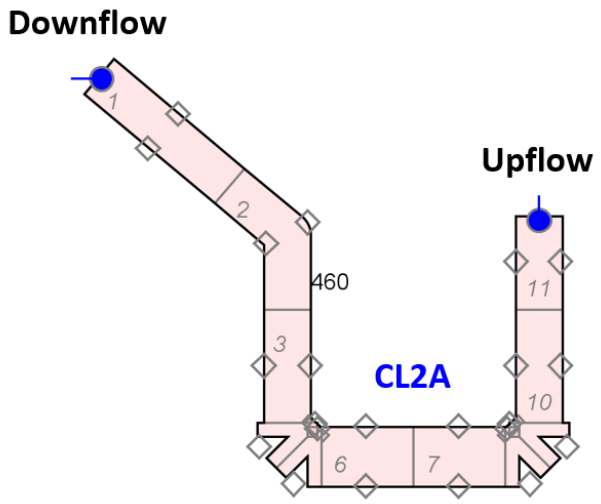

Figure 4-4 Nodalization of Intermediate Leg

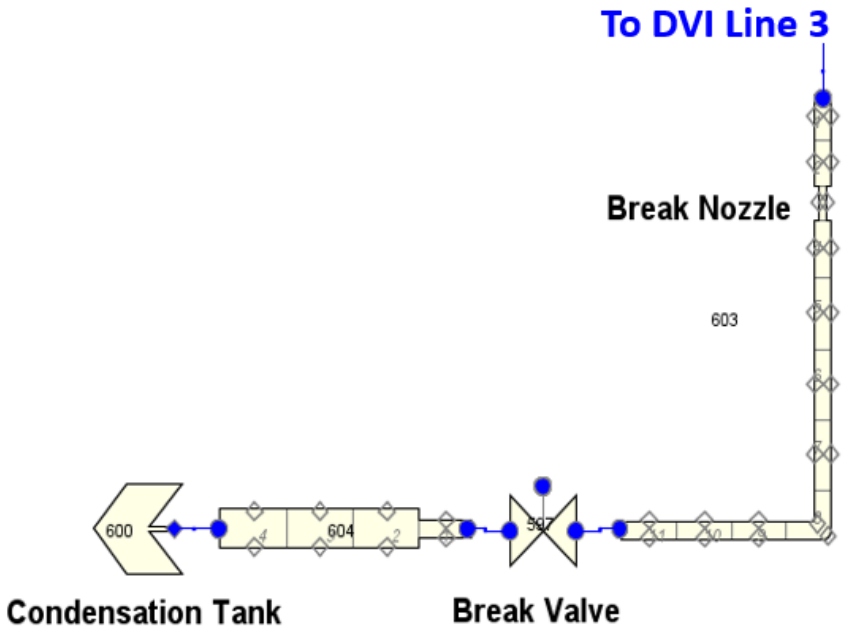

Figure 4-5 Nodalization of Break Piping System

5 STEADY-STATE CALCULATION

Through the null transient calculation of TRACE, the results of steady-state calculation were derived as shown in Table 5-1. The calculation was carried out for 2000 seconds, and the important parameters shown in Table 5-1 reached saturated conditions without any further change over time. All parameters in Table 5-1 were non-dimensionalized due to the agreement of the OECD-ATLAS2 project of which the data will be confidential until the end of 2023.

The number of the calculation columns was defined as the ratio of the experimental value to the calculated value. Therefore, if this value is greater than one, it means that the calculated value is greater than the experimental value, and if it is less than one, it means that the calculated value is smaller than the experimental value. The error was defined as the percentage of the calculated value minus the experimental value divided by the experimental value. For example, if the error is negative, it means the calculated value is smaller than the experimental value.

To determine whether the steady-state condition was reached, the measurement uncertainty provided in the experimental report [8,11] and the general acceptance criteria presented in the TRACE PWR Modeling Guidance [17] were compared with the calculation results. In the primary system, there were no errors in the normal power, the PZR pressure, or the PZR level. In this study, ATLAS was modeled by considering the normal power with heat loss. The iterative calculations changing the heat loss in the RPV and the SGs were carried out to find the optimal value. As a result of the iterative calculations, the determined net power considered the heat loss in the calculation was 0.39% less than the experiment, which is slightly greater than the maximum measurement uncertainty for the electric power of 0.35% [11]. However, for the core inlet and outlet temperatures, the calculation predicted a lower temperature than the experiment. The difference between the experiment and calculation exceeded the criteria of TRACE guidance but was lower than the measurement uncertainty. Therefore, it seems that the core inlet and outlet temperatures also reached a steady-state condition. The CL flow rate also had some errors, but it was sufficiently satisfied within both the measurement uncertainty and the TRACE guidance. In the secondary system, the steam flow rate was found to exceed the criteria of the TRACE guidance. Since the secondary system is balanced between the water supply and the steam discharge at the steady-state condition, the steam, and the feedwater flow rate should indicate the same value. It is generally known that the measurement uncertainty for the steam flow rate is much greater than for the incompressible water flow rate. Although the steam flow rate overestimated the acceptance criteria of the TRACE guidance, the feedwater flow rate was successfully satisfied with the TRACE guidance as the value was within 0.2%. Therefore, it was determined that the flow rate of feedwater and steam in the secondary side has reached the steady-state condition of the experiment. There were no errors in the feedwater temperature, the steam pressure, and the secondary side level as the level of the SGs. Although there was an error of 0.4% in the estimation of the steam temperature, the error of the stream temperature was satisfied within the measurement uncertainty. Finally, there was no error in the SIT level. So, overall, it was confirmed that all parameters successfully reached the steady-state condition under the balanced condition between the primary and secondary systems.

Table 5-1 Results of Steady-State Calculation

Parameter	Exp.	Cal.	Error (%)[1]	Measurement Uncertainty	TRACE PWR Modeling Guidance
Primary system					
Normal power (-)	1.0	1.0	0.0	± 0.35%	0%
Net power (-) (With heat loss)	1.0	0.9961	-0.39	± 0.35%	
PZR pressure (-)	1.0	1.0	0.0	± 0.039 MPa	±0.103 MPa
Core inlet temperature (-)	1.0	0.996	-0.4	± Max. 2.4K	± 2K
Core outlet temperature (-)	1.0	0.996	-0.4	± Max. 2.4K	± 2K
Cold leg flow rate (-)	1.0	0.997	-0.3	± 13~15%	± 5%
PZR level (-)	1.0	1.0	0.0	± 0.18 %	± 0.25 m
Secondary system					
Steam flow rate (-)	1.0	1.073	7.3	-	± 5%
Feedwater flow rate (-)	1.0	1.002	0.2	-	± 5%
Feedwater temperature (-)	1.0	1.0	0.0	± Max. 2.4K	0%
Steam pressure (-)	1.0	1.0	0.0	-	±0.103 MPa
Steam temperature (-)	1.0	0.996	-0.4	± Max. 2.4K	± 2K
Secondary side level (-)	1.0	1.0	0.0	-	± 0.25 m
SIT level (-)	1.0	1.0	0.0	-	

1. Error (%) = (Calculation-Experiment) / Experiment * 100

6 RESULTS AND DISCUSSION

6.1 Sequence of Events

Table 6-1 indicates the sequence of events. Time was divided by an arbitrary value and non-dimensionalized. At first, the break at the DVI line 3 was initiated by opening the valve at the break piping system. Due to the rapid decrease in the pressure of the primary system, the reactor was tripped coincident with the signal of the LPP. The MSIV and MFIV were closed with a several seconds delay after the LPP signal, sequentially. Since the steam pressure in the secondary system exceeded 8.1 MPa, the MSSVs opened at each SG and started to repeat the opening and closing for a while. The decay heat started with 12 seconds delay after the reactor trip. Then, the safety injection from the SIP-1 was initiated with dozens of seconds delay after the trip, which reflected the startup and electrical bus loading time for the Emergency Diesel Generator (EDG). Although the emergency core cooling water was supplied into the core, the core level kept decreasing and reached the minimum level. The accumulated pressure in the core was released by the occurrence of the Loop Seal Clearing (LSC). However, the core level was still low enough to induce an increase in the cladding temperature. Then, the Maximum Cladding Temperature (MCT) occurred, and the core was quenched by the continuous supply of cooling water. The SIT-1, 2, and 4 were actuated at a similar timing. The flow rates in the SITs were reduced by the valve actuation simulating the fluidic device in the APR1400. The SITs were terminated due to the emptiness of the tank. Overall, the calculation predicted very similar event times for most major sequences and the time difference between the experiment and the calculation appears to be small. Among them, the operation timing of the SIP and the timing of MCT predicted by the calculation was the same as the experiment. However, for the prediction of the core quenching time, there was the largest deviation between the experiment and the calculation. the calculation predicted a much slower core recovery than the experiment. The reason for this behavior will be analyzed in detail in the next chapter.

Table 6-1 Sequence of Events

Event	Nondimensional Time, t*[1]		Error (%)[2]	Remark
	Exp.	Cal.		
Break initiation	0.061	0.061	0.0	
LPP trip (Reactor trip)	0.064	0.064	-0.6	PT-PZR-01 < 10.72 MPa
MSIV close	0.065	0.065	-0.6	LPP + X sec. delay
MFIV close	0.066	0.065	-0.6	LPP + X sec. delay
MSSV opening	0.064	0.064	0.6	SG pressure: 8.1 Mpa
MSSV closing	0.076	0.075	-1.6	SG pressure: 7.7 Mpa
Decay heat start	0.067	0.066	-0.6	~12 sec. after reactor trip
Safety injection from SIP	0.070	0.070	0.0	LPP + XX sec. delay
The minimum water level in the reactor core	0.078	0.077	-0.3	Minimum of LT-RPV-01
Loop seal clearance	0.079	0.079	0.3	
Maximum of the cladding temperature	0.082	0.082	0.0	
Quenching of the reactor core	0.083	0.089	7.7	
Safety injection from SITs	0.108	0.103	-4.8	PT-DC-01 < 4.03 MPa
Activation of the fluidic device (SIT-1,2,4)	0.231	0.227	-2.0	Avg. of 3 SITs
Termination of SIT injection (SIT-1,2,4)	0.868	0.873	0.6	Avg. of 3 SITs
End of test	1.0	1.0	0.0	

1. t* is defined as the nondimensional time that was divided by an arbitrary value
2. Error (%) = (Calculation-Experiment) / Experiment * 100

6.2 Transient Calculation

The normal core power is shown in Figure 6-1. When comparing the experiment and calculation, the normal core power was exactly consistent from the steady state to the occurrence of the break, and after the occurrence of the break where the decay curve was applied.

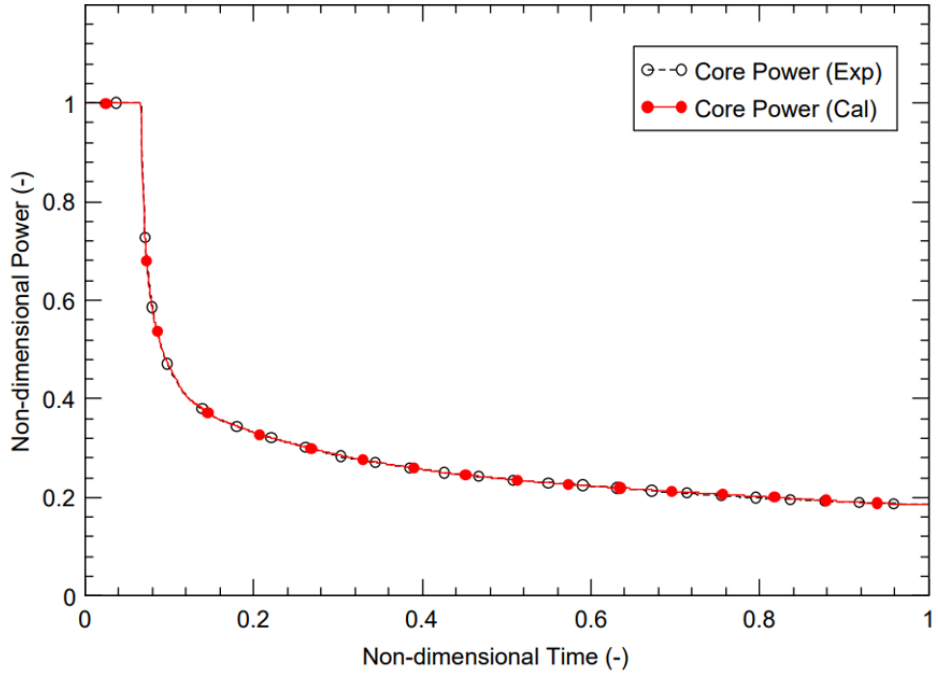

Figure 6-1 Normal Core Power

Figure 6-2 presents the choking flag showing whether the choked flow occurs in TRACE. The choked flow occurred in the DVI line 3 and the number 1 valves of the MSSVs at each SG. The choked flow for the DVI line occurred immediately after the break and continued until the LSC and the occurrence of the MCT without the release of the choked flow. As the pressure of the RPV decreased after the SIT injection, the maintenance or release of the choked flow was repeated in the DVI line. The MSSVs were opened when the secondary pressure reached 8.1 MPa and repeated to open and close for dozens of seconds. When the MSSVs were opened, the choked flow was maintained. The timing of MSSV opening and closing predicted in the calculations was similar to what observed in the experiment.

Figure 6-3 indicates the pressures in the RPV and the SGs. The RPV pressure decreased rapidly after the break, and it went through a plateau when the pressures of the RPV and the SGs became similar. If the RPV pressure became lower than the SG pressure, the reverse heat transfer from the SGs to the RPV occurred. In the primary system, a liquid-dominant two-phase flow was formed before the plateau, and a vapor-dominant two-phase flow was formed after the plateau. A decrease in the coolant level in the downcomer changed the break flow from a liquid-dominant two-phase flow to a vapor-dominant two-phase flow. The primary system pressure decreased steeply again after the end of the plateau region [8,13]. In the region of the liquid-

dominant two-phase flow, the calculation predicted a similar pressure drop to the experiment. The calculation well-predicted the plateau where the primary and secondary pressures became similar, but a more rapid pressure drop in the calculation was predicted in the region of the steam-dominant two-phase flow that occurred after the plateau. This kind of relatively over-estimated pressure drop occurred again in the latter phase of the event, which was marked with the red box. In the secondary system pressure, the pressure of SG2 was slightly higher than the pressure of SG1 in the experiment, however, the pressures of SG1 and SG2 were almost identical in the calculation. The pressures calculated in SG1 and SG2 were included in the minimum and maximum pressure ranges measured in the experiment. According to the experimental report [8], it was addressed that the different pressures of two SGs was attributed to the different amount of reverse heat transfer and the heat loss to an atmosphere. Therefore, different SG pressures in the experiment caused different heat losses through the outer wall of the SG, but the symmetrical heat losses through the SG occurred in the calculation due to a similar pressure prediction of the SG.

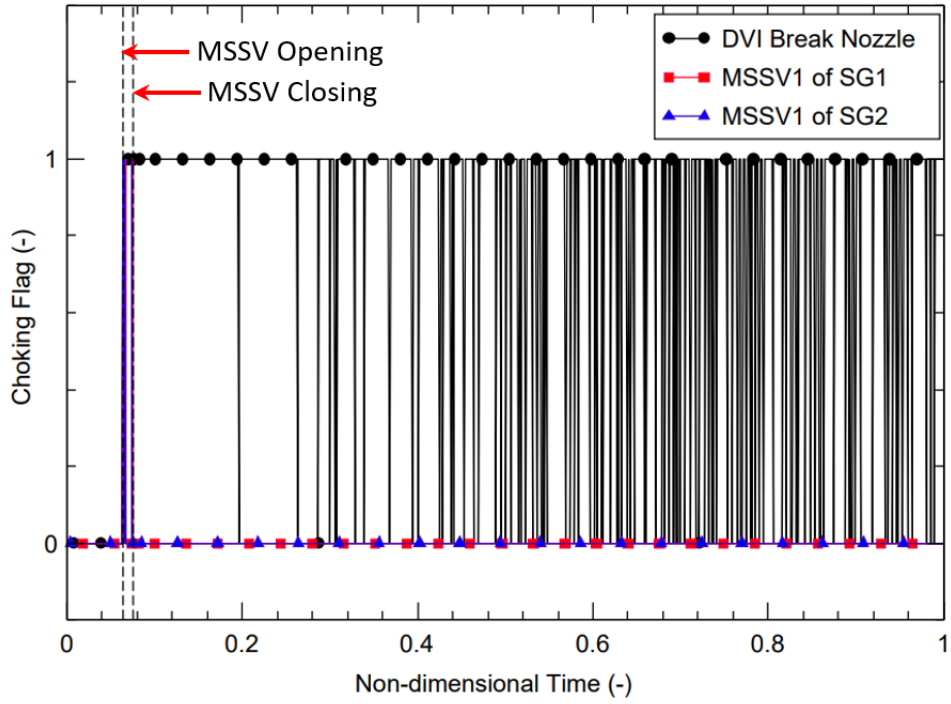

Figure 6-2 Choking Flag

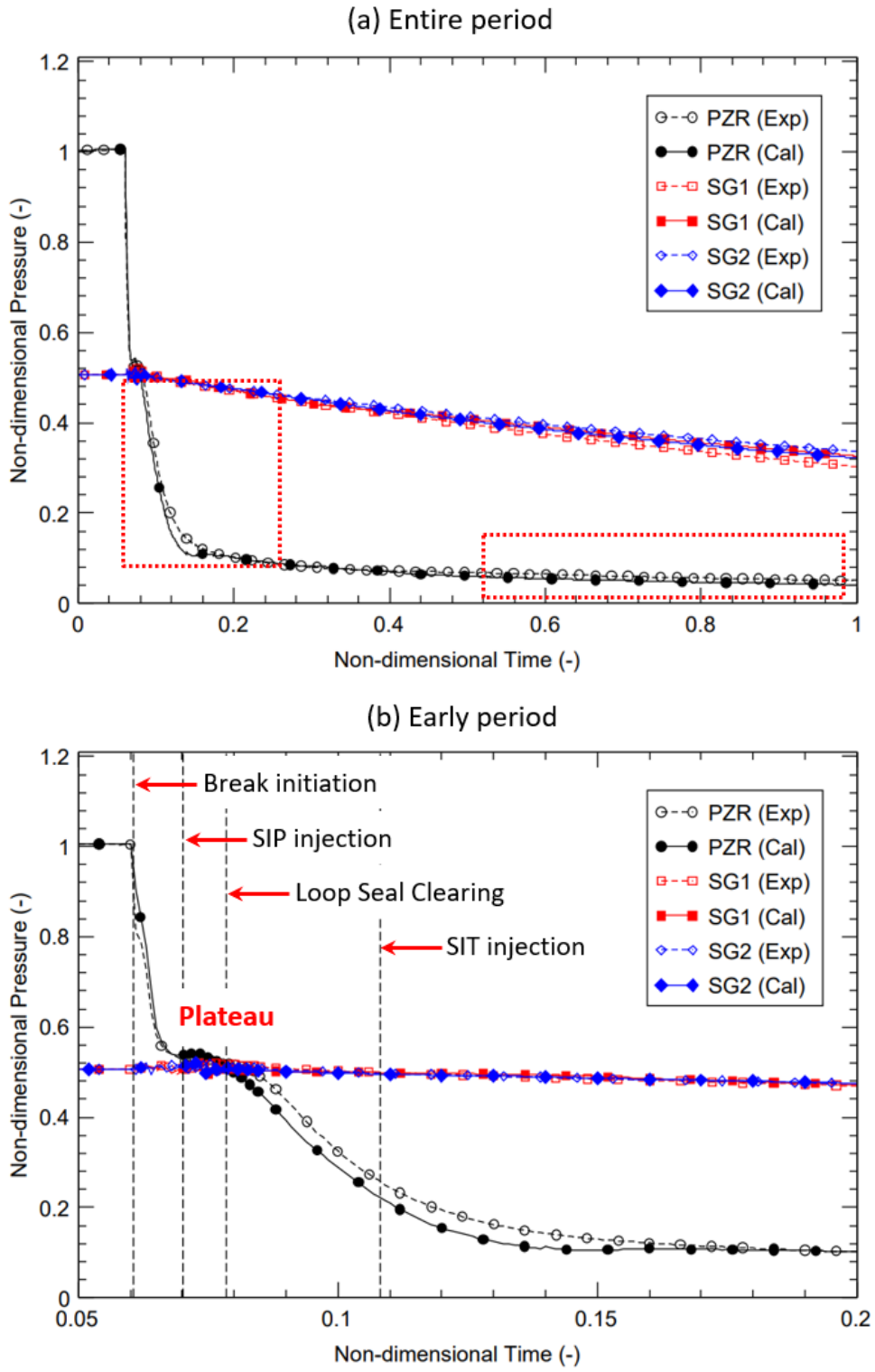

Figure 6-3 RPV and SG Pressures

Figure 6-4 shows the integrated mass of discharge flow for the DVI line and the MSSVs. The accumulated break flow of the DVI line predicted in the calculations generally agreed well with the experiment. Especially, the break flow before LSC and MCT in the calculation was in good agreement with the experiment. However, after SIT injection, the calculated break flow was lower than in the experiment. Regarding the break flow of MSSVs, since the calculation predicts a similar opening and closing behavior to the experiment that occurs at the beginning of the event, the calculation was well-matched with the experiment. Through this analysis, it confirmed that the choked flow modeling for the DVI line and MSSVs were appropriate to simulate the overall behavior of the discharge flow in the test.

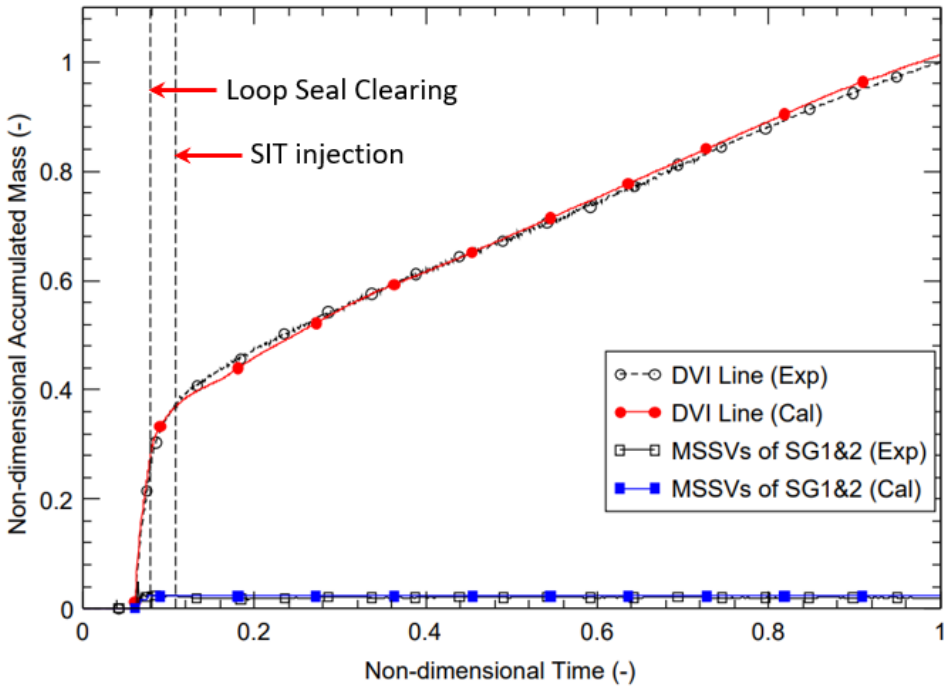

Figure 6-4 Integrated Mass of Discharge Flow

Figure 6-5 presents the mass flow rate in SIPs. The SIP-1 was only operated but the SIP-3 wasn't. The calculation properly predicted the timing of the SIP injection and the overall injection flow rate similarly to the experiment. However, since the SIP was modeled by a performance curve modeled as primary system pressure versus the flow rate and the calculation predicted the lower RPV pressure than the experiment as shown in Figure 6-3, the calculation over-predicted the SIP flow rate when a vapor-dominant two-phase flow occurred at the early phase.

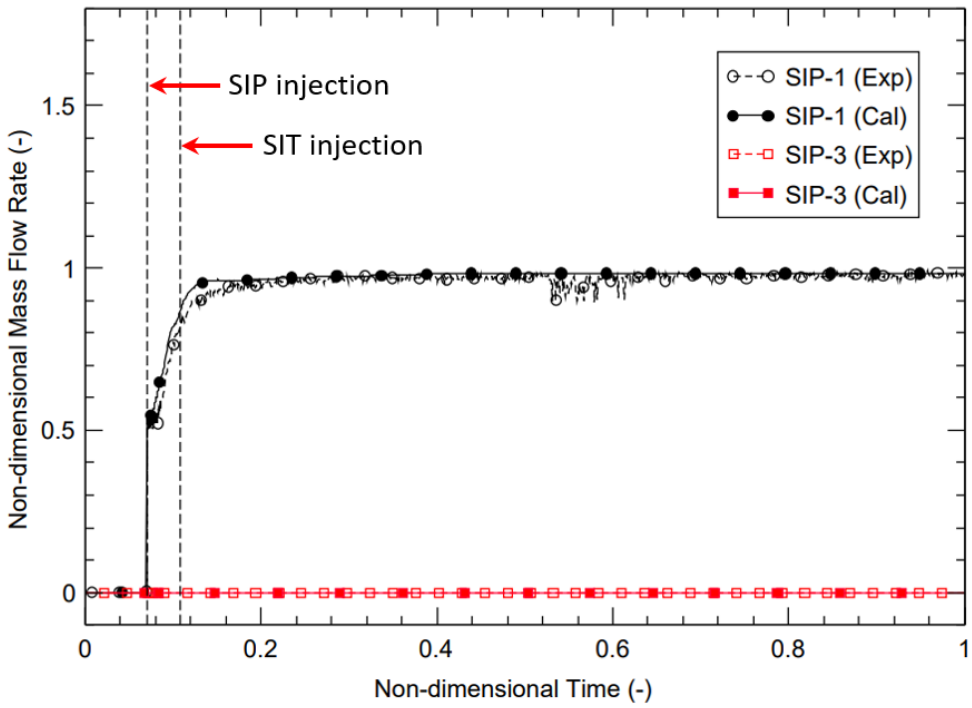

Figure 6-5 Mass Flow Rate of SIPs

Figure 6-6 shows the mass flow rate of four SITs. The SIT-1, 2, and 4 were operated. The predicted injection timings were similar to the experiment in all SITs. The predicted overall flow rate was well-matched with the experiment. However, the calculation over-predicted the flow rate at the early phase of the injection because the predicted RPV pressure was lower than the experiment. The flow rate of SITs was changed at around t*=0.23, which is the averaged operation timing of the fluidic device. The flow pattern was changed from the high flow to the low flow based on t*=0.23. Looking at the termination timing of SITs, the predicted timing of each SIT did not correspond one-to-one with the measured timing. Although the termination timing of each SIT was different from the experiment and the calculation, the predicted overall termination behavior was similar to the experiment because the calculation predicted a certain SIT having a different number was terminated in a timely manner.

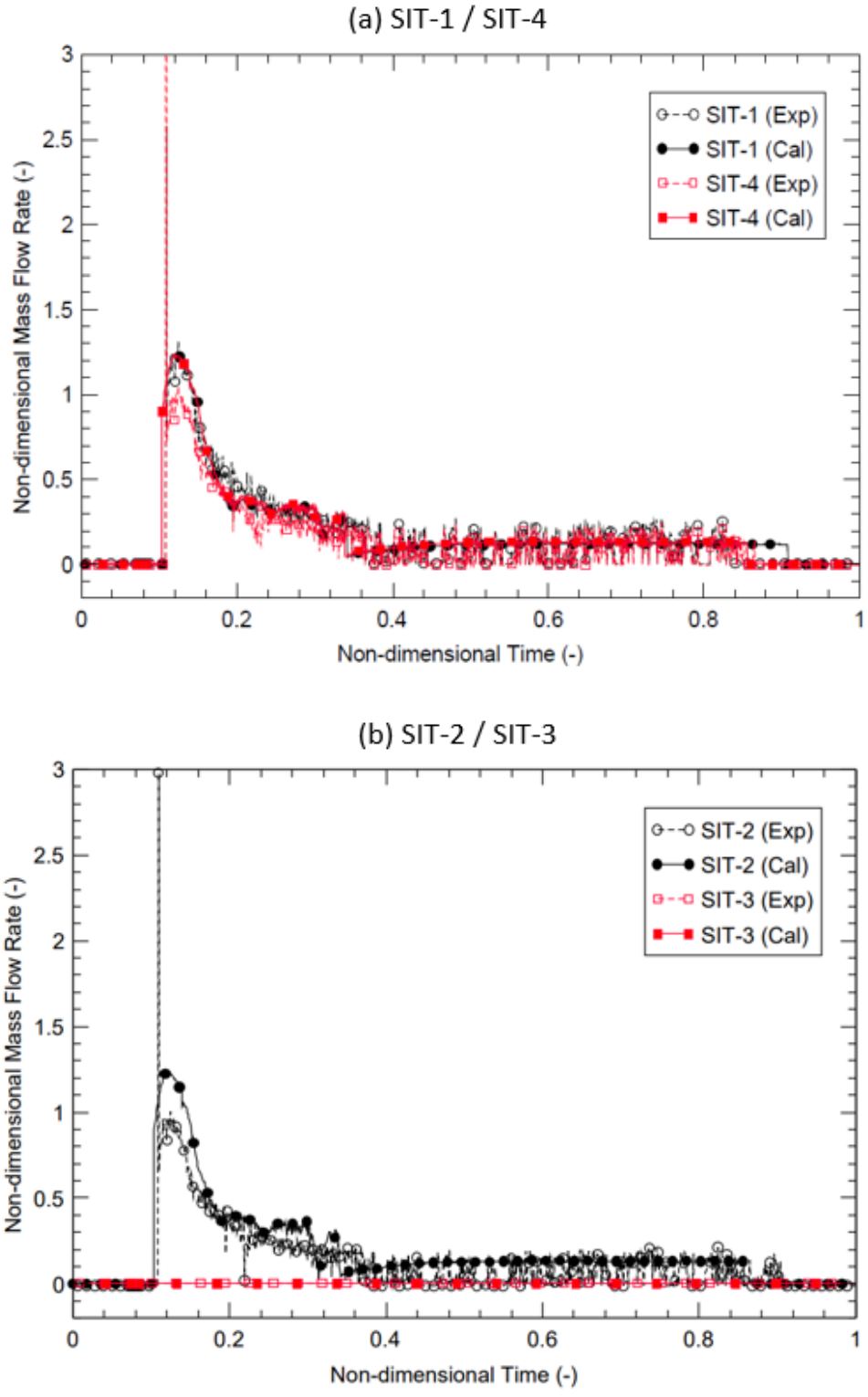

Figure 6-6 Mass Flow Rate of SITs

Figures 6-7 present the collapsed water level in SG1 and SG2. The water level of the SGs showed a similar level in calculations and experiments until the time when LSC and MCT occurred. However, after the rapid pressure drop of the RPV that occurs after the plateau, the calculation predicted a clearly lower water level than the experiment. To compensate for this difference, the control models of TRACE for the estimation of the collapsed water level in SGs were improved, but the tendency of under-prediction of the water level was not improved.

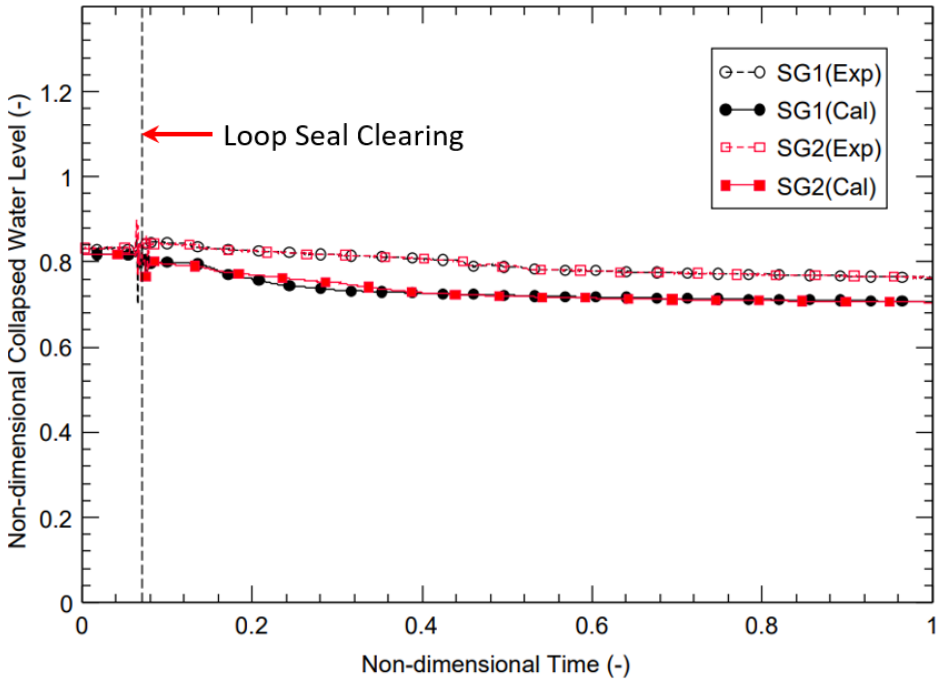

Figure 6-7 Collapsed Water Level in SG1 and SG2

Figure 6-8 indicates the collapsed water level in SITs. The water level change for the three SITs observed at the experiment was similar to each other, and the calculation predicted a similar behavior to the experiment from the beginning to the end of the injection.

Figure 6-9 shows the mass flow rate of HLs. The calculation well-simulated the peak flow rate at the early phase and the gradually increasing oscillating flow rate due to the steam condensation in HLs. The calculation also relatively well-captured the maximum and minimum of the flow observed in the experiment.

Figure 6-10 presents the mass flow rate of CLs. The calculation adequately simulated the peak flow rate at the beginning of the break in the four CLs observed in the experiment and the tendency of the sudden decrease of the flow rate due to the exhaustion of coolant in the core. After the middle of the event, the oscillation of the flow rate occurred in the experiment, but zero flow rate was observed without oscillation in the calculation.

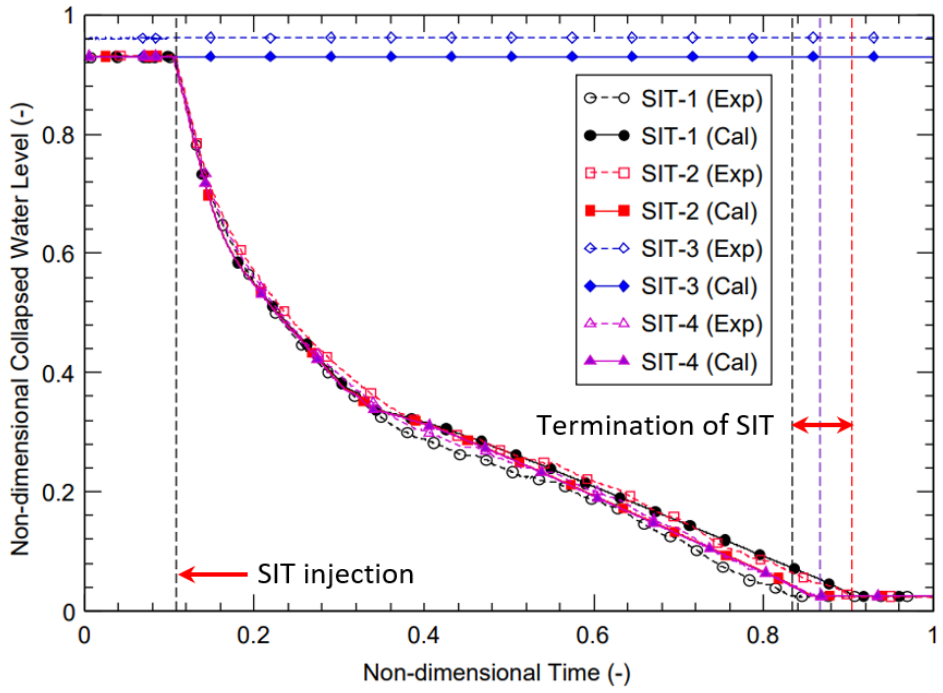

Figure 6-8 Collapsed Water Level in SITs

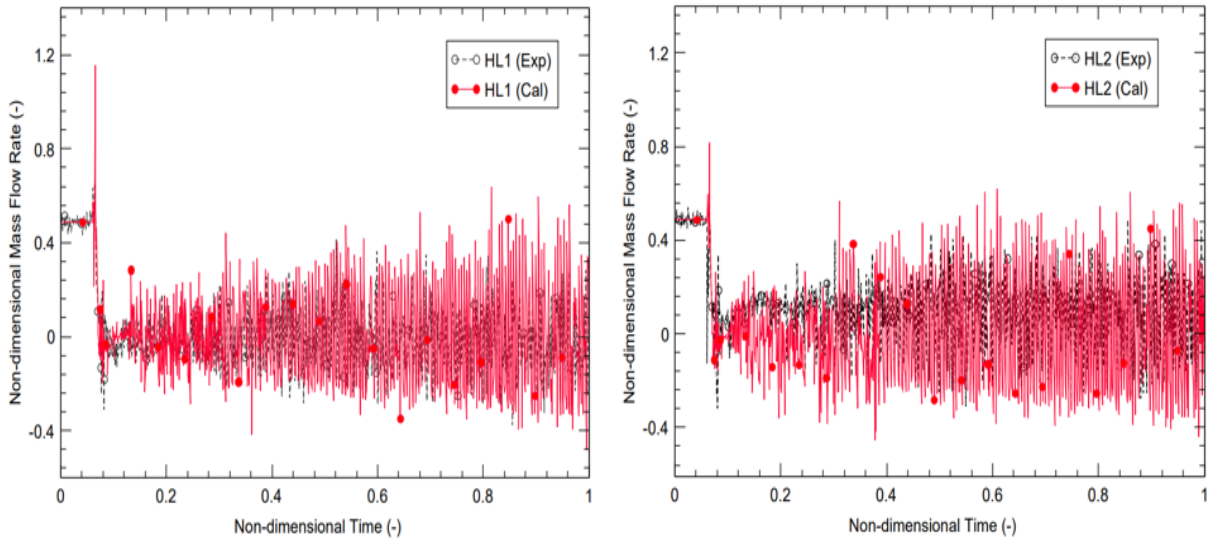

Figure 6-9 Mass Flow Rate of Hot Legs

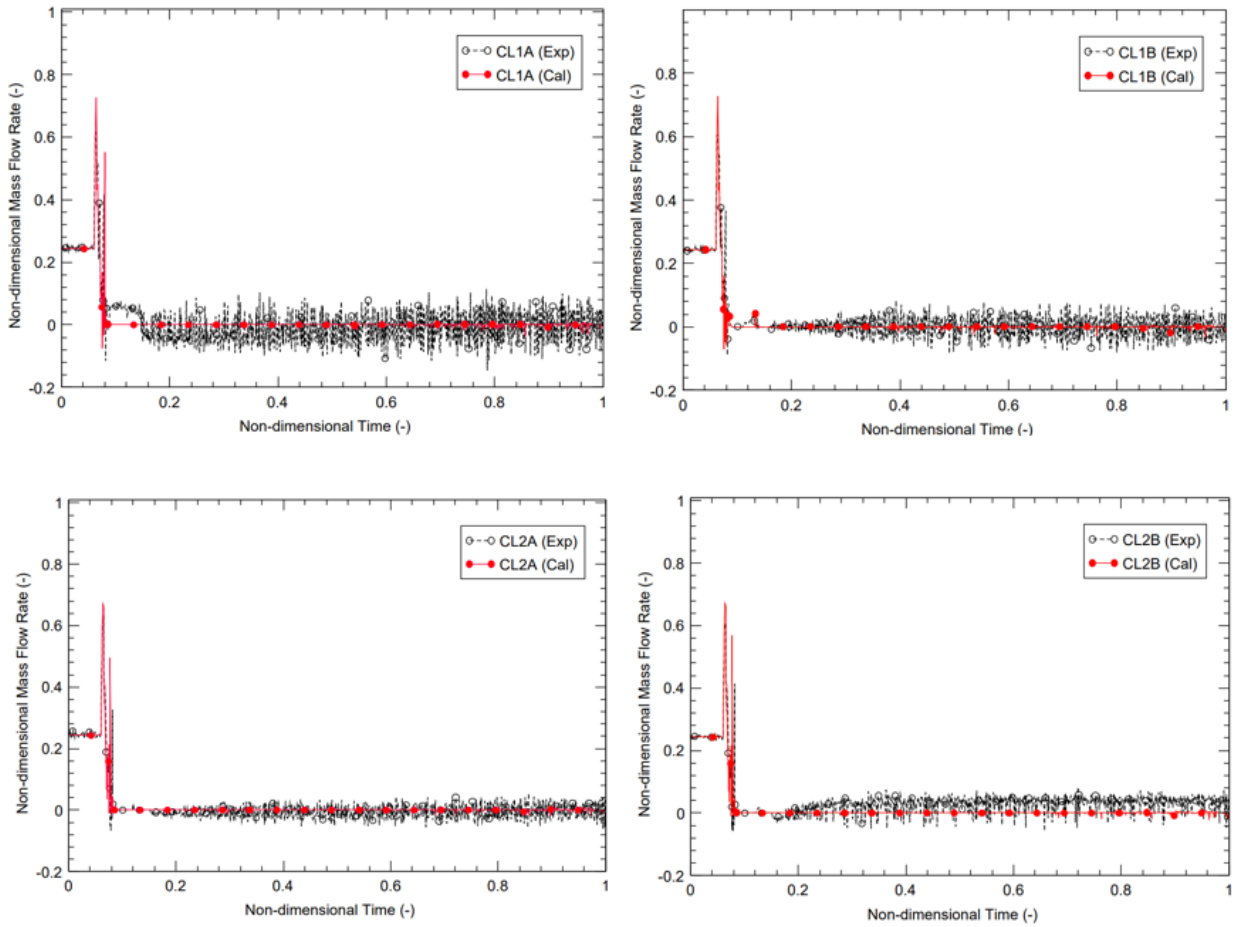

Figure 6-10 Mass Flow Rate of Cold Legs

Figure 6-11 shows the collapsed water level of intermediate legs. As shown in Figure 4-4, the intermediate legs can be divided into the upflow piping entering the core and the downflow piping connected to the SG side, and the calculation results for each region are shown in Figure 6-11. In most of the intermediate legs, the calculation seemed to simulate well the rapid decrease in water level due to the occurrence of LSC at a similar time as the experiment. However, in the calculation, there was a definite delay in the water level decrease in the Upflow of CL 1B and a sudden recovery of the water level in the Downflow of CL 1B after the depletion of the water. These delays in the calculation affected the core cooling rate after MCT occurred and caused the delayed core quenching time.

Figure 6-12 presents the MCT. The calculation accurately predicted the same MCT at the same timing as the experiment. According to the effect that the predicted pressure of RPV rapidly decreased after the plateau, the calculation predicted a lower temperature than the experiment at the time from t* = 0.06 after MCT to t*=0.17 and from t* = 0.5 to t* = 1.0. This is because when the RPV pressure is lower than the experiment, the corresponding saturation temperature becomes lower and the temperature of the surrounding region serving as a heat sink adjacent to heater rods also can be decreased. So, more heat loss in the heater rods can result in decreased cladding temperature.

Specifically, looking at the MCT predicted by the calculation and the heater group where the MCT occurred, the predicted MCT was the same as the experiment, but the predicted heater group where the MCT occurred was different from the experiment. In the experiment, MCT occurred in G3, which is the outermost region of the core, but in the calculation, MCT occurred in the innermost region, G1. According to the experiment report [8], it was stated that a smaller flow or cooling capability in the outer region of the core might cause MCT to appear in the outermost region in the experiment.

On the other hand, in order to find the reason why the MCT position is different between the experiment and the calculation, the local behavior predicted by the calculation where the MCT occurred was analyzed. It was confirmed that the local mass flow rate through the G3 channel was twice that of the G1 channel and the heat transfer coefficient of the G3 region was twice as high as that of the G1 region in the calculation. The difference in local behavior predicted by the calculation and measured by the experiment resulted in different locations of MCTs. The measured cladding temperatures were high in the order of G3, G2, and G1 groups in the experiment. However, the predicted cladding temperatures were high in the order of G1, G3, and G1 groups.

(a) Upflow

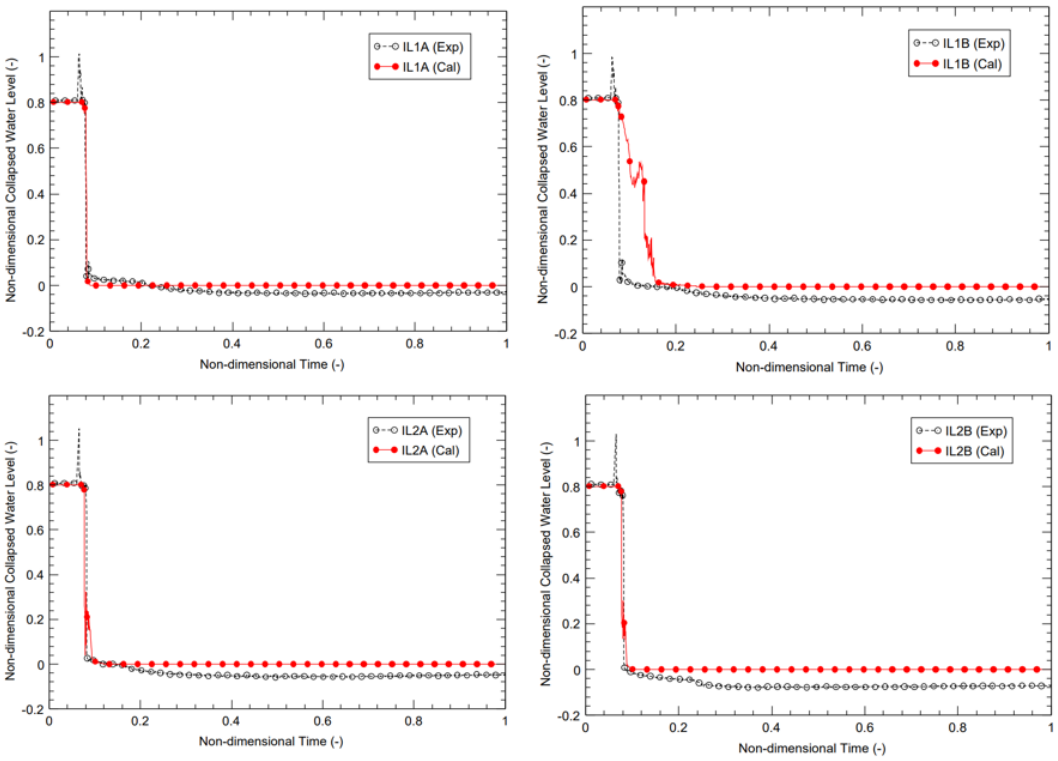

(b) Downflow

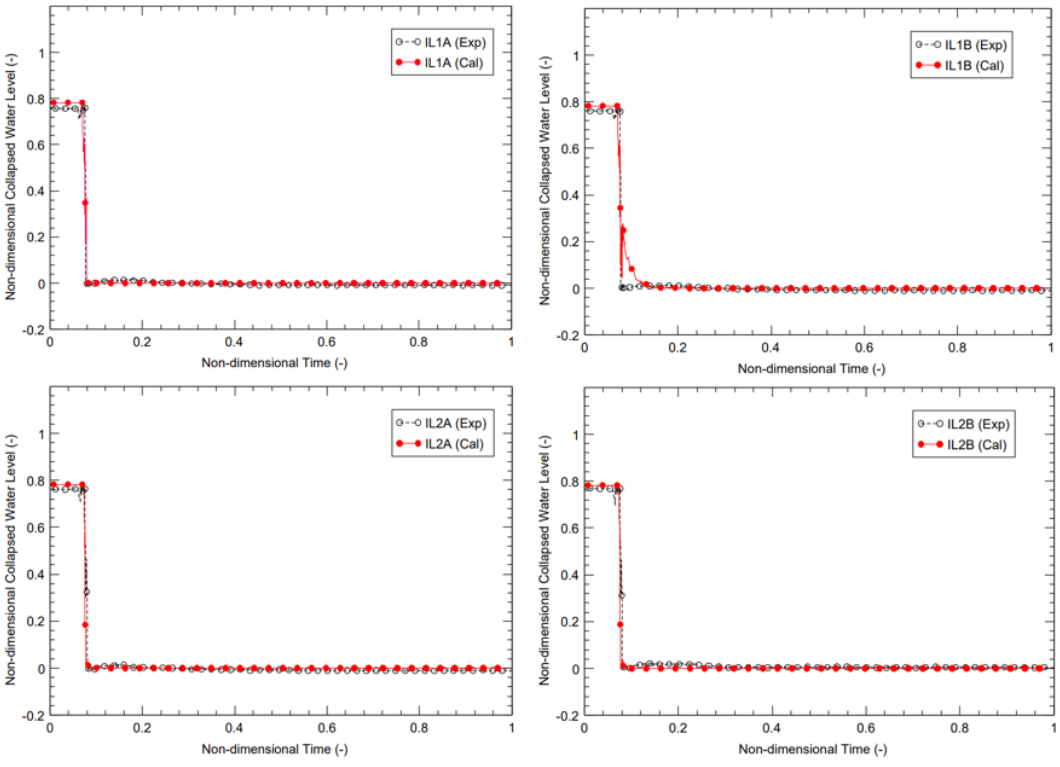

Figure 6-11 Collapsed Water Level of Intermediate Legs

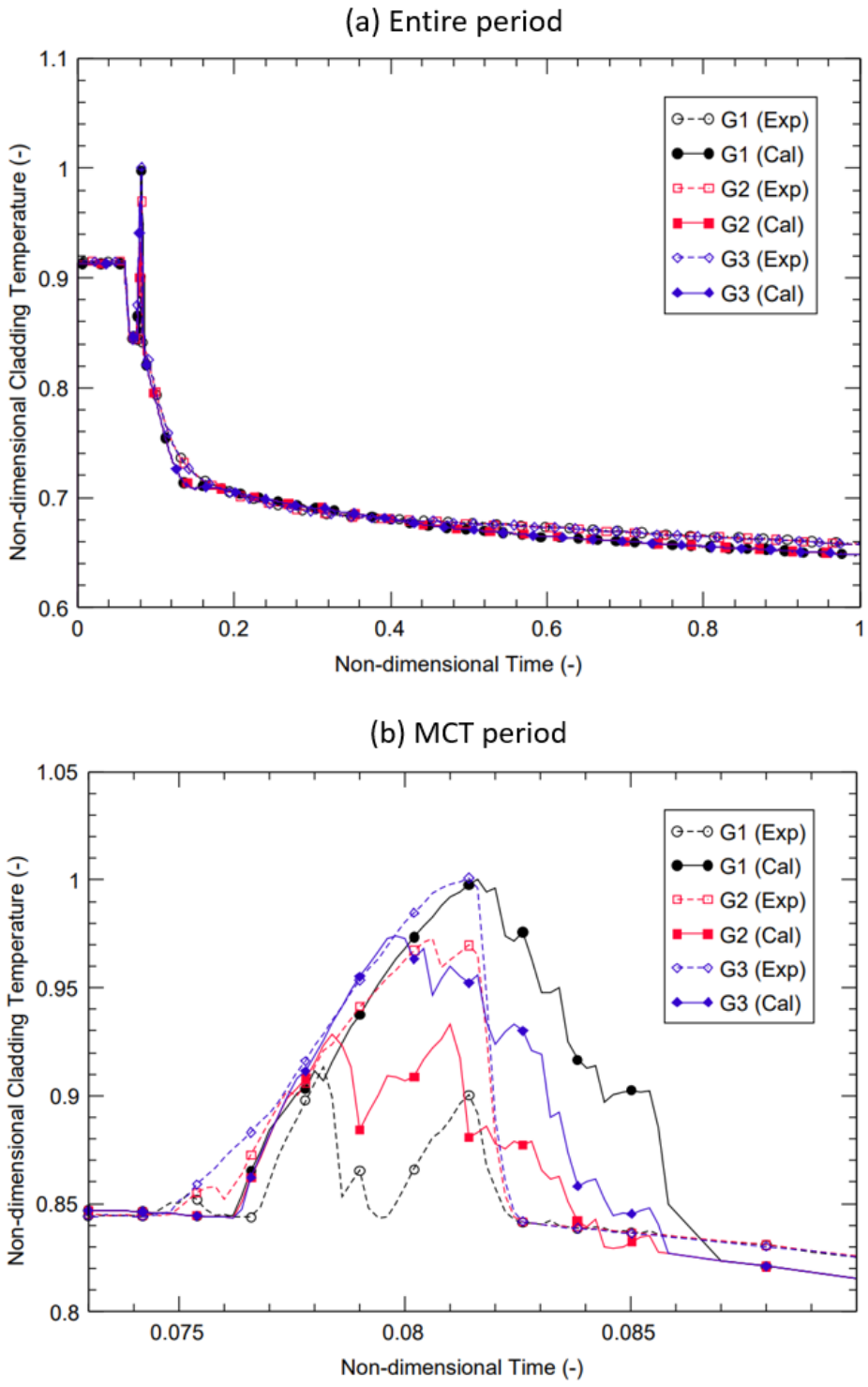

Figure 6-12 Maximum Cladding Temperature

Figure 6-13 indicates the collapsed water level of the core and downcomer. This figure also shows the maximum measurement uncertainty with an error bar, which is presented in the experimental report [8]. The calculation well-predicted the minimum water level that occurred in the core and downcomer after the break and its timing. Regarding the water level recovery, the predicted speed of the water level recovery in the downcomer was similar to or a little faster than the experiment, but the water level recovery in the core proceeded later than the experiment. In addition, the finally saturated levels in both the core and the downcomer were predicted to be somewhat lower than the maximum measurement uncertainty. As is generally known, the timing of minimum level in the core and MCT occurrence are closely related. Figure 6-14 shows the relation between MCT and the collapsed water levels of the core and the intermediate leg 1A. Comparing the MCT behavior of the experiment and calculation, Although the heater groups were different, the calculation predicted a similar heat-up behavior with the same MCT as the experiment but a delayed cool-down time or core quenching. The reasons for the delayed core quenching in the calculation are considered as follows. First, the calculation for the level of the intermediate leg 1A predicted a later LSC than the experiment, which is shown as blue lines in Figure 6-14. The LSC in the intermediate leg 1A appeared to occur at a similar timing to the experiment in Figure 6-11, but when expanded to the timeline where MCT occurs, it was confirmed that the calculation for LSC was slower than the experiment. And as shown in Figure 6-13, since the predicted LSC in the intermediate leg 1B was more delayed than that in the intermediate leg 1A, the overall predicted LSC in the entire legs could be much more delayed than the experiment. As a result of the delay of LSC in the multiple intermediate legs, the predicted recovery of the core water level, which occurs after the LSC, was also delayed compared to the experiment, resulting in a delayed core quenching.

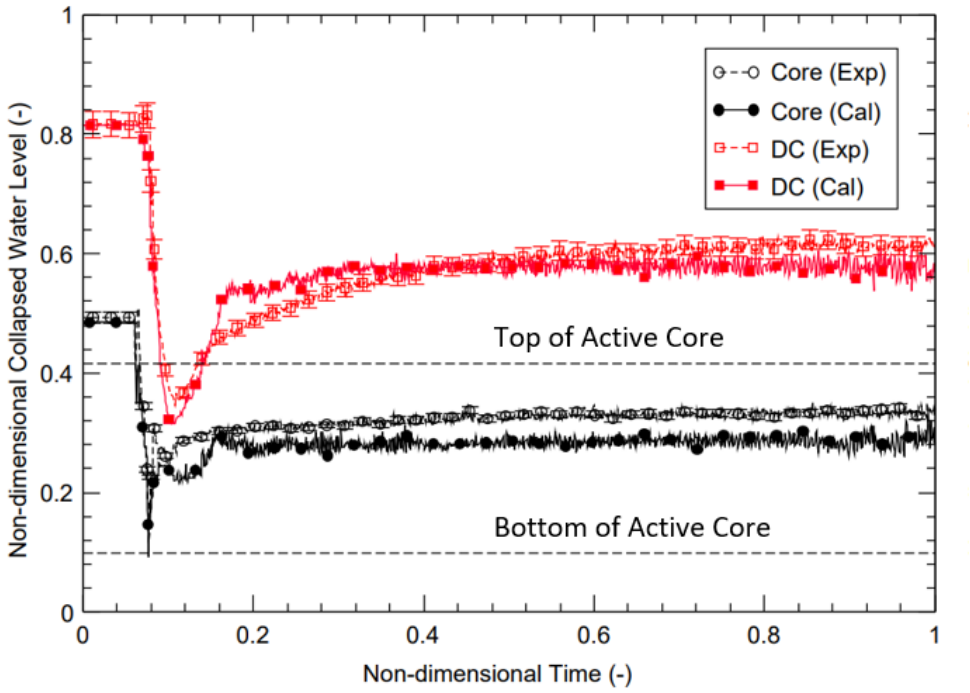

Figure 6-13 Collapsed Water Level of Core and Downcomer

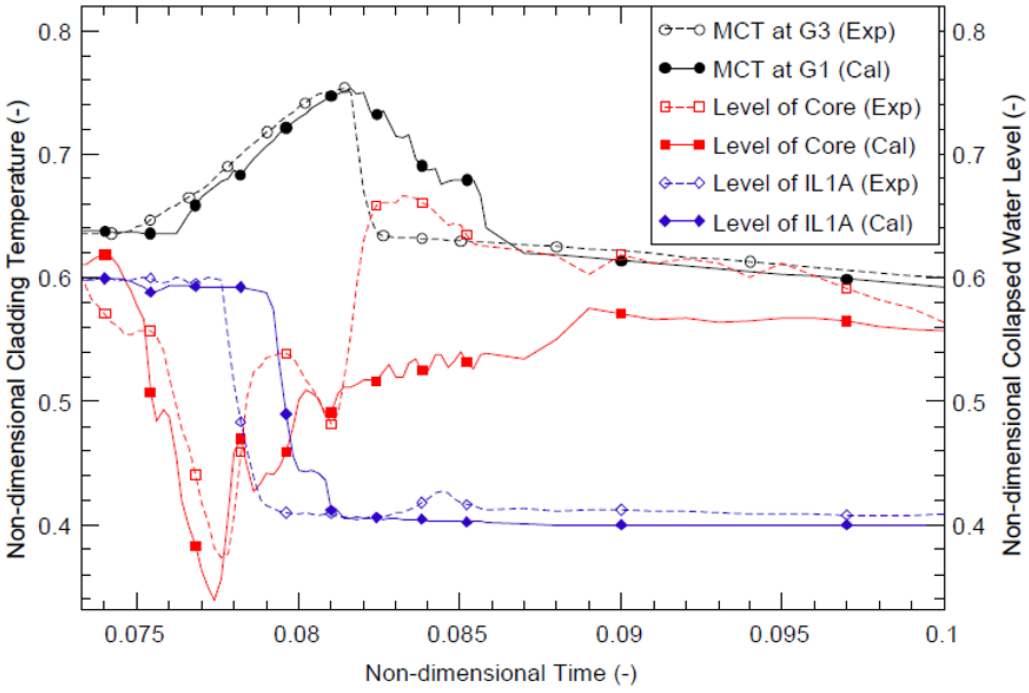

Figure 6-14 Cladding Temperature and Collapsed Water Level

6.3 Sensitivity Studies

6.3.1 Break Size

According to previous studies, although the ATLAS2 B3.1 and B3.2 tests were both tests for IBLOCA, no excursion of cladding temperature occurred in the PZR surgeline break (B3.1 test) simulating a 10-inch break of APR1400, and a large increase in cladding temperature was observed in the DVI line break (B3.2 test) simulating an 8.5-inch break [12]. This result means that in the IBLOCA scenario, there may be a break position that is sensitive to an increase in the cladding temperature.

Sensitivity studies were carried out for the break size in the DVI line break in which a high cladding temperature rise occurred despite the break size being smaller than the B3.1 test. Assuming arbitrary break sizes, the thermal-hydraulic behavior and the effect on the cladding temperature were investigated. The 100% break size of DVI line 3 was set as the base case, and the sensitivity studies for the break size were performed by changing the area of the break nozzle as shown in Table 6-2. However, except for the break size, parameters such as discharge coefficients of the Ransom-Trapp model, CCFL options, and hydraulic and thermal components were all kept the same.

Table 6-2 Sensitivity Studies for Break Size

Name	Model Description
BS-DVI Line-50%	50% break area at DVI line 3
BS-DVI Line-100%	Base case (100% break area at DVI line 3)
BS-DVI Line-200%	200% break area at DVI line 3
BS-DVI Line-300%	300% break area at DVI line 3

Figure 6-15 shows the integrated mass of discharge flow at different break sizes. It can be seen that as the break size increases, more coolant on the primary side was discharged. Figure 6-16 indicates the pressure of RPV. The RPV pressure decreased more rapidly in the case where there was a large discharge flow through the break, and the plateau period in which the primary and secondary pressures equilibrate was also shortened.

Figure 6-17 presents the secondary discharge flow through MSSVs. Contrary to the reduction in coolant inventory through the DVI line, as the break size increased, the discharge flow through the secondary side MSSVs decreased. This was because the total amount of heat transferred from the primary to the secondary system decreased due to the rapid decrease in the coolant inventory in the primary side, and there was not enough heat to continuously repeat the opening and closing of the MSSV.

Figure 6-18 shows MCT according to the break size. MCT did not occur in the case where the break size was 50%, but MCT occurred in all other cases. And as the break size increased, the MCT tended to increase. This cause can be explained through the collapsed water level in the

core shown in Figure 6-19. The larger the break size, the faster the core water level decreased and the lower the minimum core water level. In addition, it took more time to recover the core level after the core uncover due to the same SIP coolant supply despite of the different break sizes. A 100% break and a 200% break predicted a similar minimum water level, but the 200% break had more coolant discharge than the 100% break, so it took longer to recover the core level. Since the heater continued to rise in temperature until the core level was recovered, the MCT was higher in the case of a 200% break than in the case of 100%, even though a similar core level was predicted. Through the results of this sensitivity study, it was confirmed that when the break size of IBLOCA increased at the same break position, the cladding temperature generally increased in proportion to the break size.

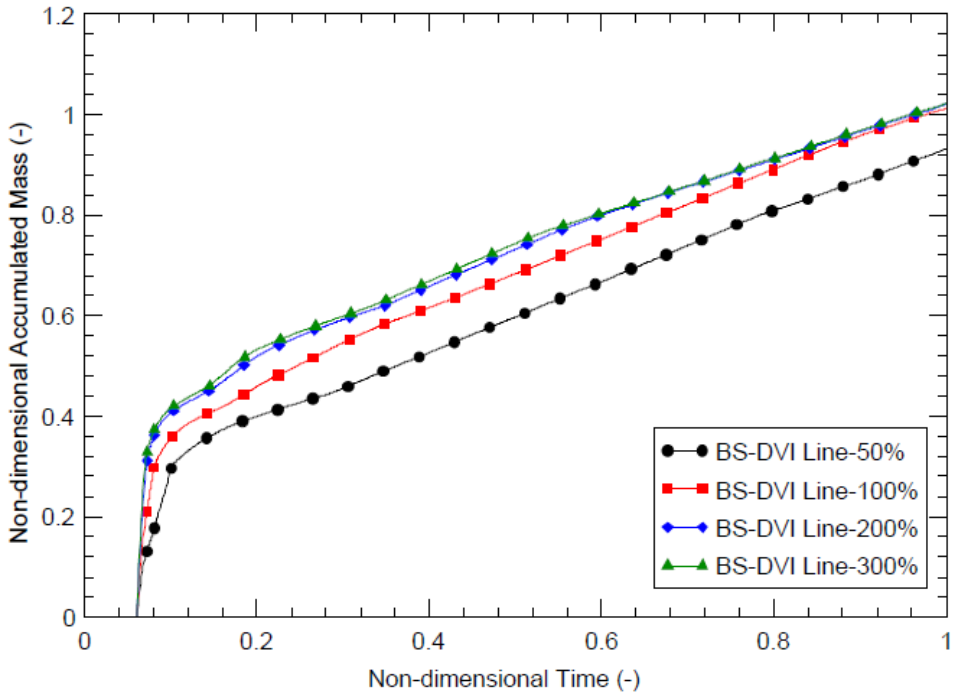

Figure 6-15 Integrated Mass of DVI Discharge Flow at Different Break Sizes

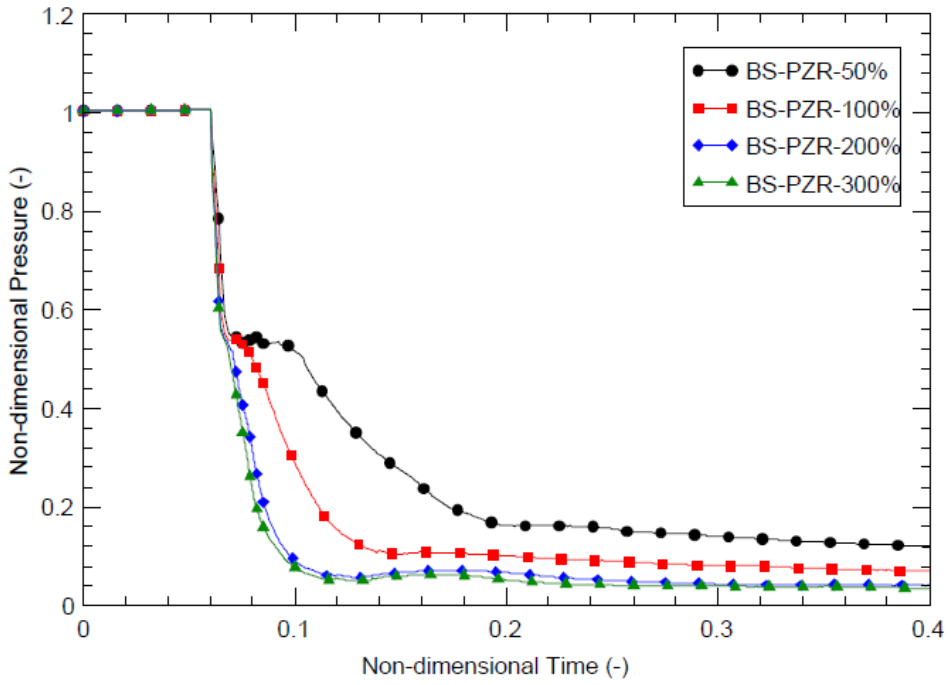

Figure 6-16 RPV Pressure at Different Break Sizes

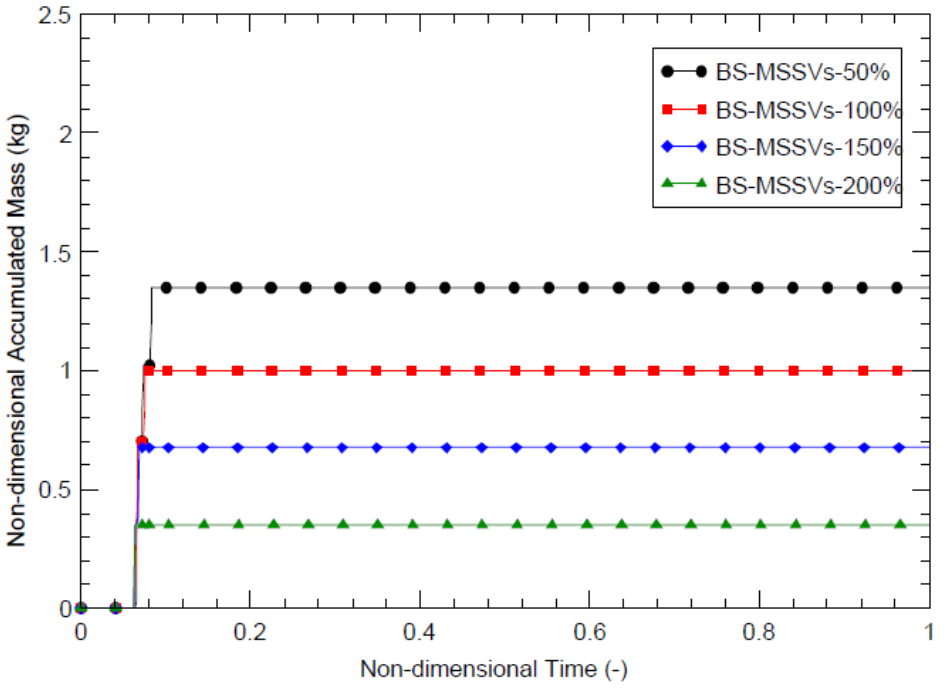

Figure 6-17 Integrated Mass of MSSV Discharge Flow at Different Break Sizes

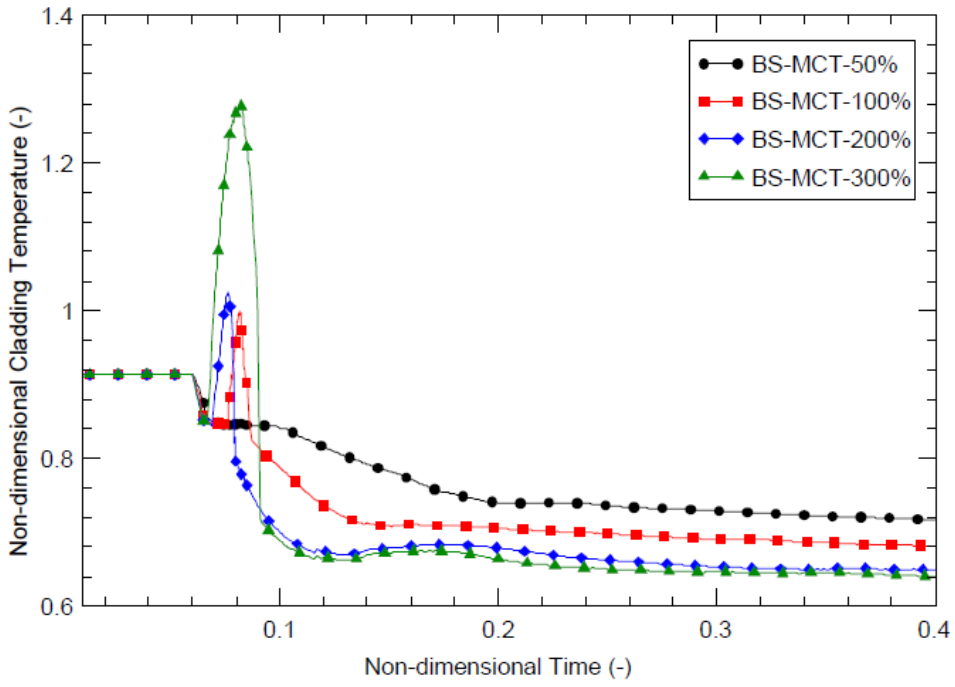

Figure 6-18 Maximum Cladding Temperature at Different Break Sizes

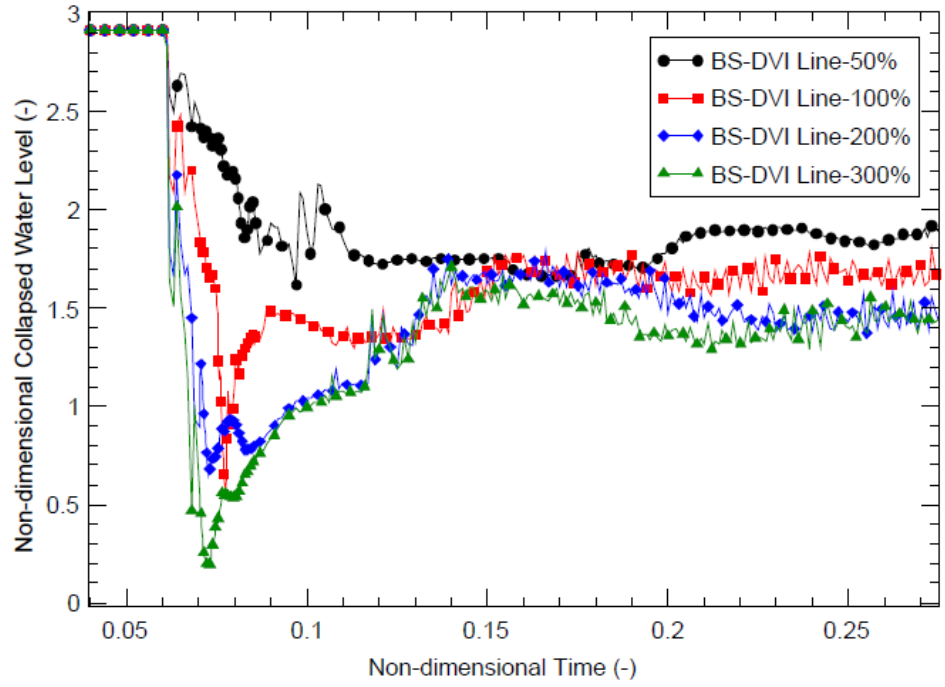

Figure 6-19 Collapsed Water Level of the Core at Different Break Sizes

6.3.2 Break Position

Two types of sensitivity studies were performed as shown in Table 6-3 by changing the break position and single failure assumption under the condition of the same break size. The first is the conservative case in which the same single failure assumption for the EDG operation as the base case was applied and the break location was only changed, and one SIP and three SITs were operable. The second, unlike the base case, assumed a non-conservative assumption of an EDG failure, in which two SIPs and three SITs were operable.

Table 6-3 Sensitivity Studies for Break Position

Conservative Assumption	
Name	**Model Description**
BP-DVI Line-3	Base case (Break: DVI line 3, Credited: SIP-1 / SIT-1,2,4)
BP-DVI Line-1	Break: DVI line 1 Credited: SIP-3 / SIT-2,3,4
BP-DVI Line-2	Break: DVI line 2 Credited: SIP-4 / SIT-1,3,4
BP-DVI Line-4	Break: DVI line 4 Credited: SIP-2 / SIT-1,2,3
Non-conservative Assumption	
Name	**Model Description**
BP-DVI Line-3-NC	Break: DVI line 3 Credited: SIP-2,4 / SIT-1,2,4
BP-DVI Line-1-NC	Break: DVI line 1 Credited: SIP-2,4 / SIT-2,3,4
BP-DVI Line-2-NC	Break: DVI line 2 Credited: SIP-1,3 / SIT-1,3,4
BP-DVI Line-4-NC	Break: DVI line 4 Credited: SIP-1,3 / SIT-1,2,3

The results of the sensitivity studies for the break position using the conservative assumption are as follows. Figure 6-20 shows the integrated mass of the DVI discharge flow. Since the break position was changed to different DVI lines and the discharge coefficients of the Ransom-Trapp model were kept the same, the sum of discharge flow through the DVI line was the same for all positions including the base case. As shown in Figure 6-21, the RPV pressure was not affected by the change in the break location. Figures 6-22 and 6-23 indicate MCT and collapsed water level of the core, respectively. The excursion behavior of the cladding temperature occurred in all cases, however, the highest MCT occurred in the DVI line 3. Even when the break position was only changed and the same input conditions were used, the quantitative

behavior of the cladding temperature rise was different depending on the DVI line position. Considering the position of PZR adjacent to the DVI line 3, the case of DVI line 2 was the identical case that is symmetrical to the case of DVI line 3. So, it was predicted a similar MCT each other, but the MCT of DVI line 2 was lower than that of DVI line 3, which was similar to the other cases. It is thought that a consistent behavior of the cladding temperature depending on the break position has not been confirmed because of the randomness of the LSC phenomenon. As shown in Figure 6-23, it is also thought that the reason why the highest MCT occurred in the DVI line 3 is that the case of the DVI line 3 showed the lowest minimum water level and the slowest speed of core level recovery. From a regulatory point of view, it may be necessary to check whether there is a specific break position that can cause a large increase in cladding temperature depending on the characteristics of the power plant through this sensitivity study.

Secondly, sensitivity studies for the break position using non-conservative assumptions were performed. For the cases applied for the non-conservative assumption, one additional SIP was operable compared to the base case so a total of two SIP were operated. Therefore, the discharge flow through the DVI line was different from the base case as shown in Figure 6-24 and the total amount of the discharge flow for the non-conservative cases was increased due to the effect of the additional SIP flow. As shown in Figure 6-25, although the injected mass of the SIP flow was doubled, the RPV pressure was almost the same as the base case. This was thought to be because one more SIP was operated, but the flow rate supplied to the core is not large enough to significantly change the core pressure. Figures 6-26 and 6-27 present MCT and collapsed water level of the core, respectively. As more coolant was supplied to the core, the minimum water level of RPV became higher, and the excursion behavior of the cladding temperature for all non-conservative cases was moderate. Although the injected coolant into the core was higher than the amount of one SIP flow, the cladding temperatures for the non-conservative cases were higher than those of the conservative cases which have different break positions as shown in Figure 6-22. Comparing Figures 6-23 and 6-27, although the non-conservative cases provided higher safety injection flow rates than the conservative cases, the minimum water level of the core in the non-conservative cases was predicted to be lower than the conservative cases with different break positions. Although the additional safety injection flow rate also affects the cladding temperature, more importantly, it was confirmed again that the minimum core level, which was induced by complex behaviors in the core, such as the behavior in the upper downcomer and the LSC, was the most decisive factor in determining the cladding temperature.

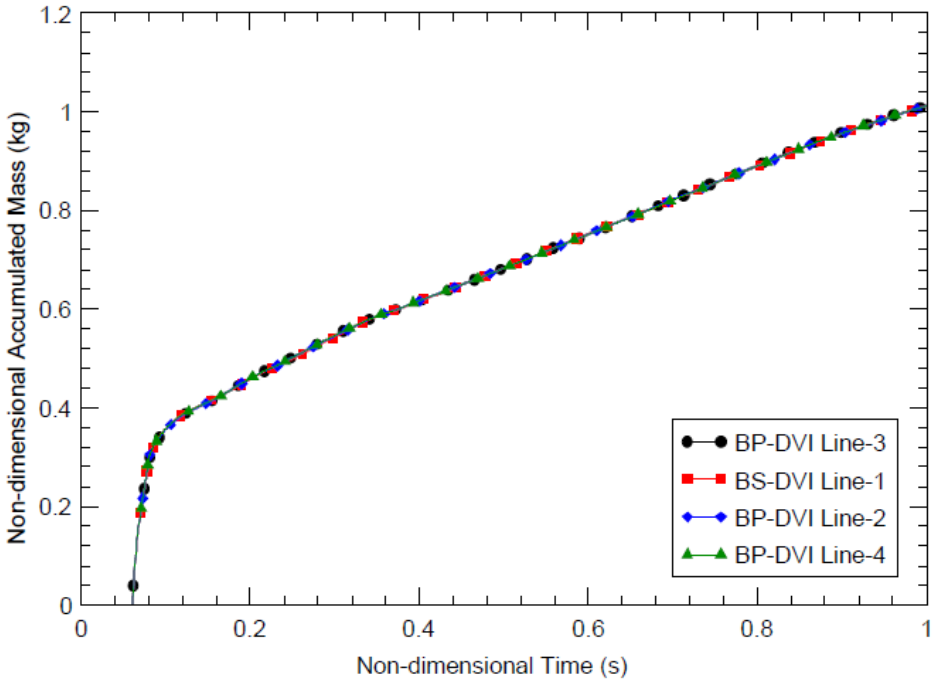

Figure 6-20 Integrated Mass of DVI Discharge Flow at Conservative Break Positions

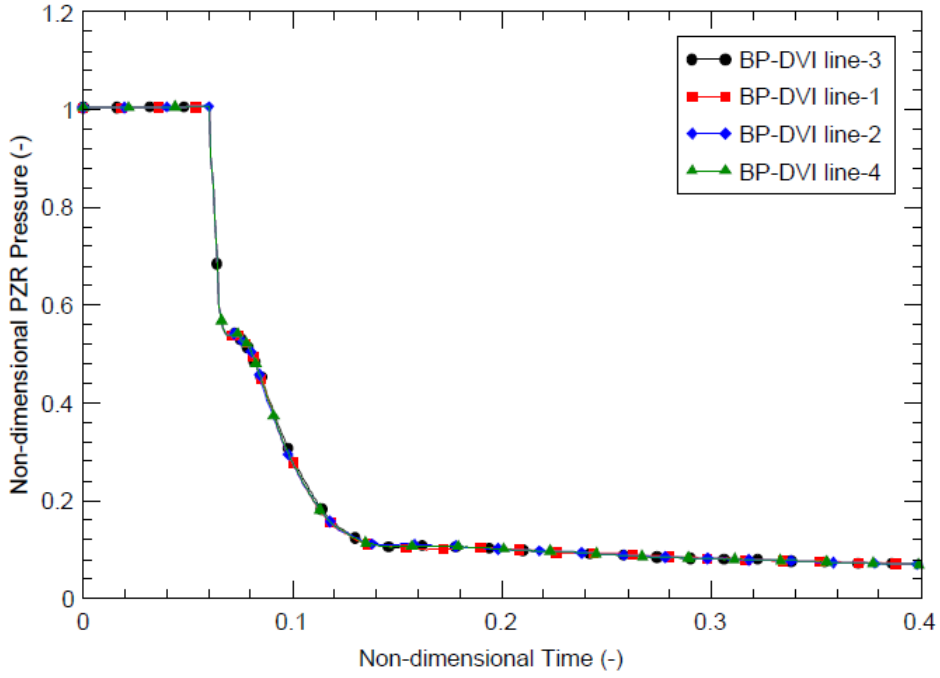

Figure 6-21 RPV Pressure at Conservative Break Positions

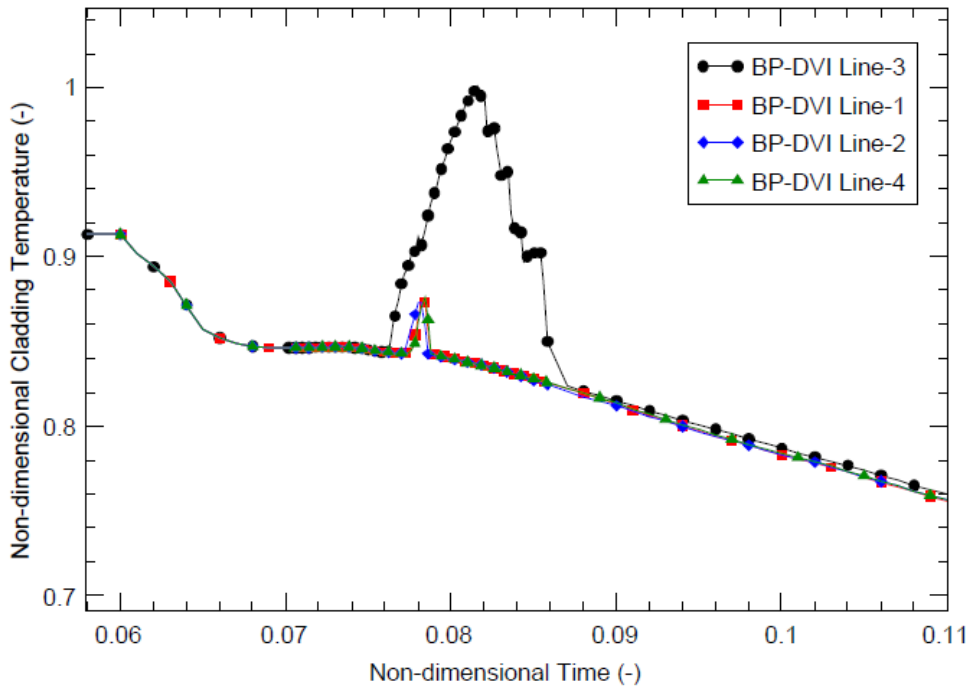

Figure 6-22 Maximum Cladding Temperature at Conservative Break Positions

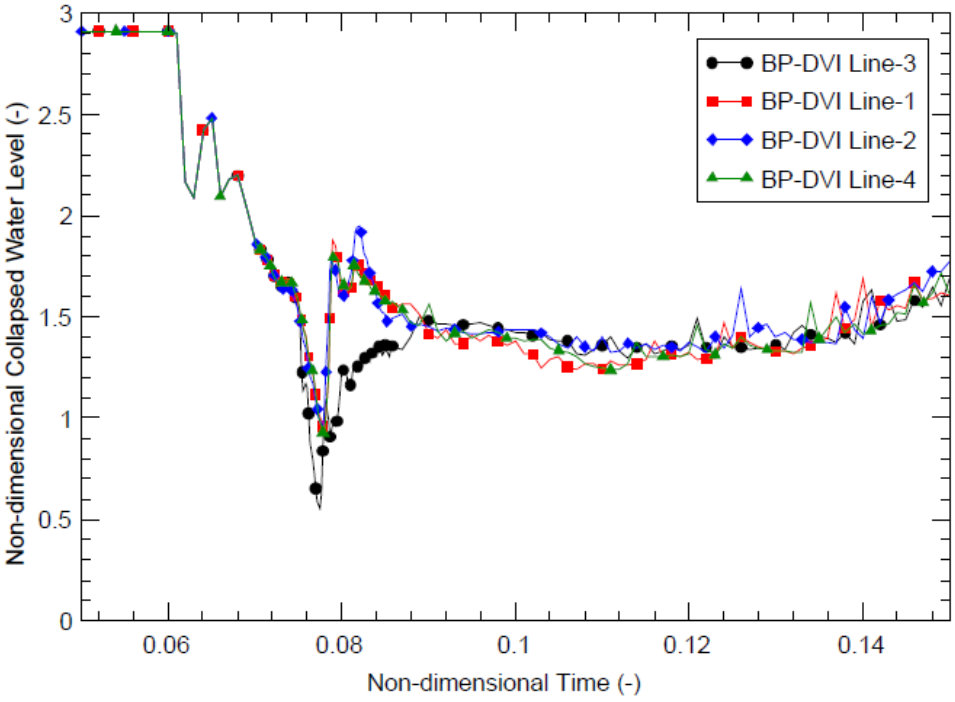

Figure 6-23 Collapsed Water Level of the Core at Conservative Break Positions

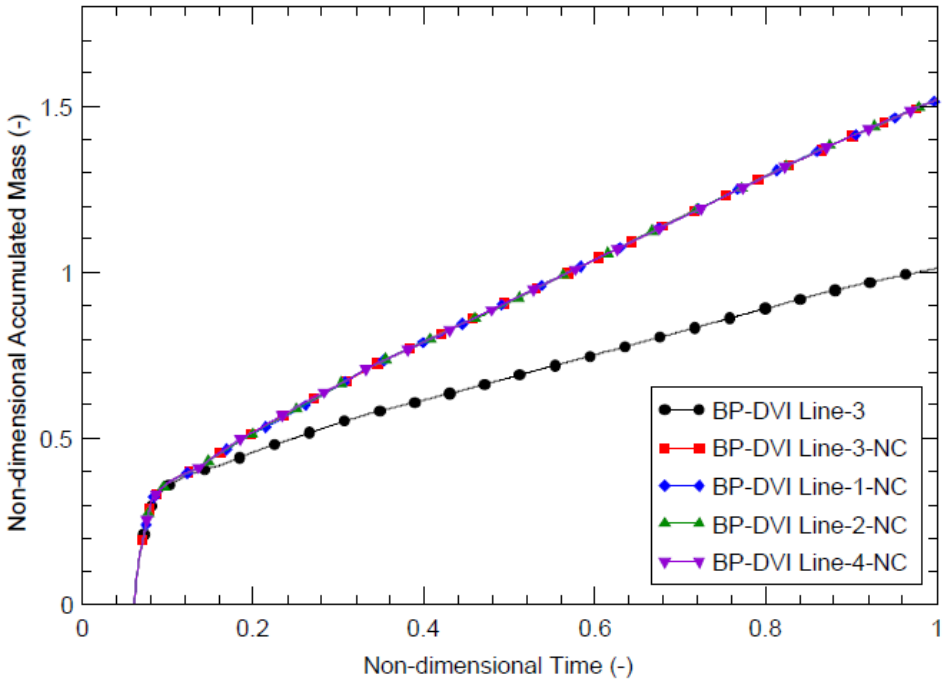

Figure 6-24 Integrated Mass of DVI Discharge Flow at Non-Conservative Break Positions

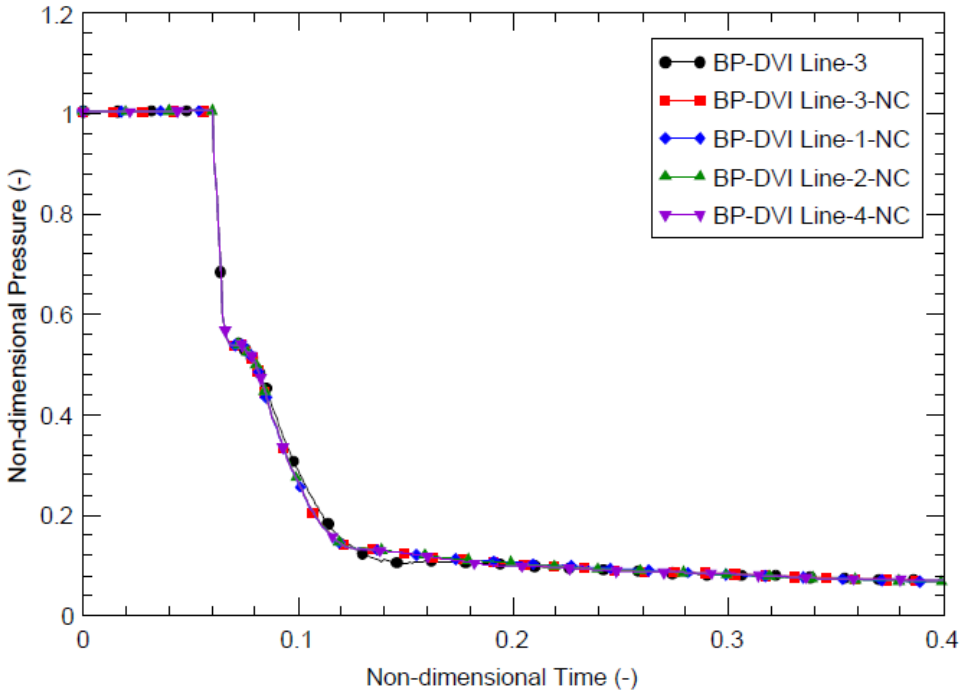

Figure 6-25 RPV Pressure at Non-Conservative Break Positions

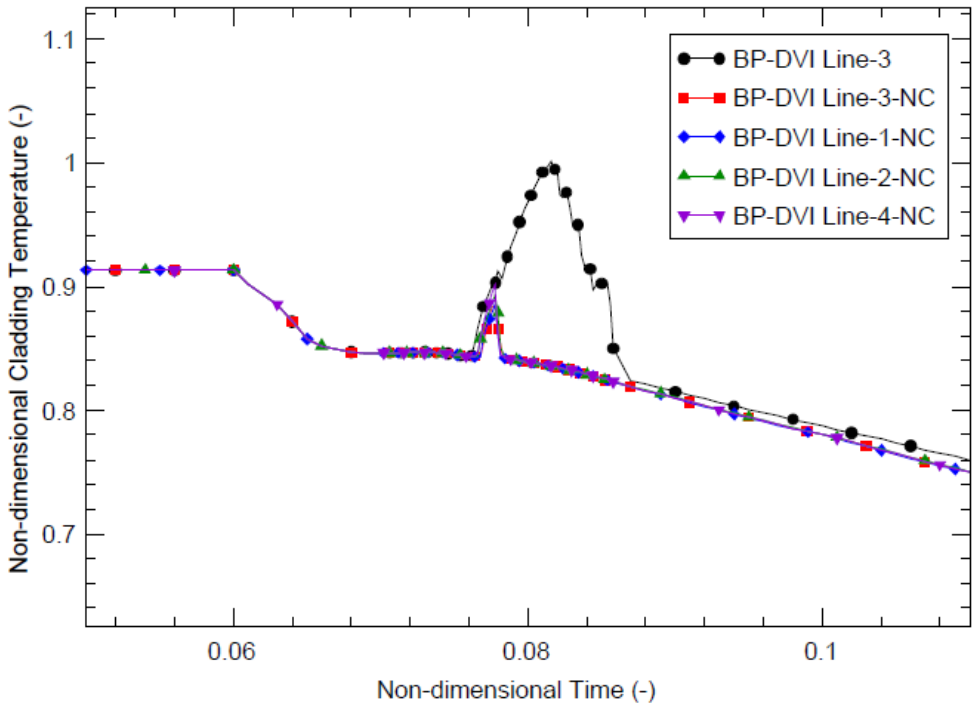

Figure 6-26 Maximum Cladding Temperature at Non-Conservative Break Positions

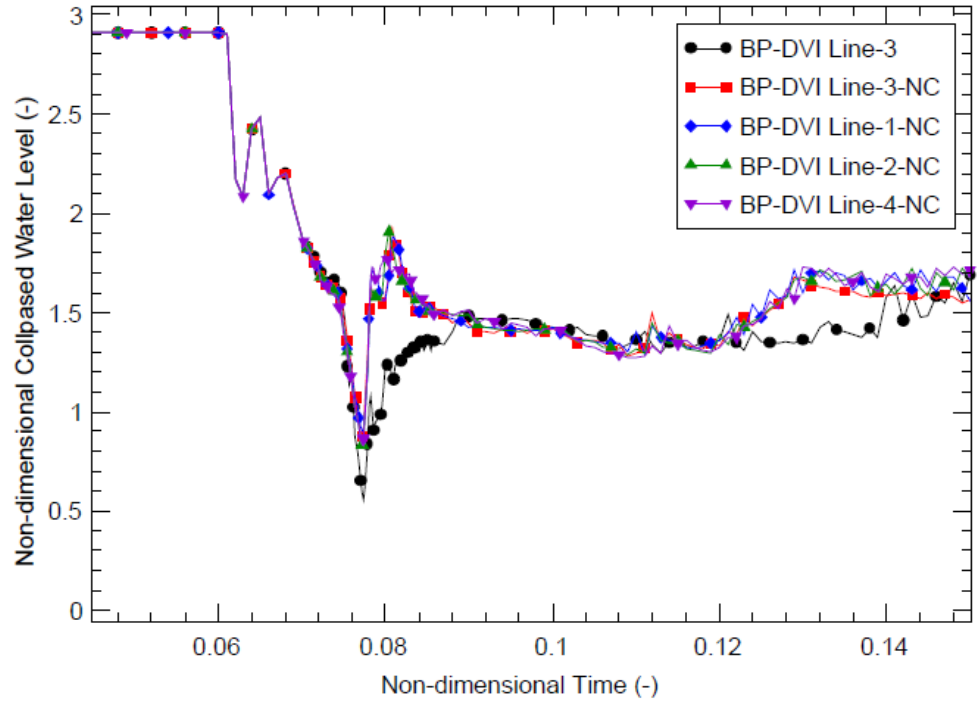

Figure 6-27 Collapsed Water Level of the Core at Non-Conservative Break Positions

7 CONCLUSIONS

The assessment of TRACE V5.0 Patch 7 was carried out using the OECD-ATLAS2 B3.2 test, which is an IET on the IBLOCA of the ATLAS facility and has an equivalent size of 100% DVI line break of the APR1400.

Regarding the TRACE input model, the RPV was modeled by a VESSEL component consisting of twenty axial levels, six azimuthal sectors, and four radial rings. The SGs with U-tubes, the HLs, the CLs, the PZR, and connecting piping were modeled by a combination of one-dimensional PIPE components. The ECCS including the SIP and the SIT with appropriate control logics, a total of 124 heat structures, and four POWER components were also modeled. To properly simulate the behavior of the LSC, the CCFL model was applied to a total of 4 regions: the Fuel Alignment Plate, Hot Leg Riser, Inlet of SG U-tubes, and Outlet of Intermediate Legs. The discharge coefficients of the Ransom-Trapp model were optimized for the break at the DVI line and the Main Steam Safety Valves.

Through the null transient calculation of TRACE, the results of steady-state calculation were derived and compared with the maximum of the measurement uncertainty and the acceptance criteria presented in the TRACE Modeling Guidance. All parameters reached the steady-state condition and were satisfied with the either of two criteria.

TRACE showed a generally good agreement with most of the sequence of events of the experiment including the opening and closing time of the MSSVs, the injection timing of the SIP and SIT, the minimum core level, and the occurrence of the LSC. However, it predicted a delayed core quenching time after the LSC. It was confirmed that the calculated total core power was the same as the experiment, including the decay curve. The predicted integrated mass of discharge flow and the mass flow rate of the SIP, SITs, CLs, and HLs were well-matched with the experiment. Although the predicted pressure drop in the RPV presented a good agreement with the experiment for the region of the liquid-dominant two-phase flow, it indicated a more rapid pressure drop than the experiment for the region of the steam-dominant two-phase flow. TRACE predicted the same MCT at the same timing as the experiment. However, the predicted position of the MCT in the heater group was different from the experiment because the local behavior predicted by the calculation was different from the experiment. Due to the delayed core level recovery and the LSC, the predicted core quenching time was delayed.

Sensitivity studies were carried out for the different break sizes and positions. As a result of the sensitivity studies for the break sizes, it was found that the cladding temperature generally increased in proportion to the break size under the condition of the same break size. Through the sensitivity studies for the break positions, it was found that there could be a vulnerable break position due to the randomness of the LSC, which may show a higher cladding temperature although the break size is the same. It was also found that the most decisive factor in determining the cladding temperature is the behavior of the minimum core level resulting from the complex behavior of the LSC and the upper downcomer rather than whether or not the additional SIP was activated.

In conclusion, TRACE showed a good agreement with the experiment for the most sequence of events and transient behaviors in the major parameters. TRACE showed an excellent capability to predict the same MCT at the same timing as the experiment. However, it showed a

reasonable capability to predict the pressure drop in RPV for the region of the steam-dominant two-phase flow, the recovery of the core level, and the core quenching time.

8 ACKNOWLEDGEMENTS

The authors would like to express the deepest gratitude to Dr. Chris L. Hoxie who supervised the program of the human resource exchange between the KINS and the NRC under the CAMP program, Mr. Ronald Harrington who served as a research mentor for the international assignee, and Dr. Joseph Staudenmeier who also served as a research mentor for this study and who reviewed this report at the NRC.

9 REFERENCES

[1] R. Tregoning, L. Abramson, P. Scott, A. Csontos, Estimating Loss-of-Coolant Accident (LOCA) frequencies through the elicitation process. NUREG-1829, U.S. Nuclear Regulatory Commission, April 2008.

[2] J.P. Poloski, D.G. Marksberry, C.L. Atwood, W.J. Galyean, Rates of Initiating Events at U.S. Nuclear Power Plants: 1987-1995, NUREG/CR-5750 (INEEL/EXT-98-00401), U.S. Nuclear Regulatory Commission, February 1999.

[3] Severe Accident Risks: An Assessment for Five U.S. Nuclear Power Plants, NUREG-1150, U.S. Nuclear Regulatory Commission, December 1990.

[4] Reactor Safety Study: An Assessment of Accident Risks in US Commercial Nuclear Power Plants, WASH-1400 (NUREG 75/014), U.S. Nuclear Regulatory Commission, 1975.

[5] S.A. Eide, D.M. Rasmuson, C.L. Atwood, Estimating Loss-of-Coolant Accident frequencies for the standardized plant analysis risk models, ANS PSA 2008 Topical Meeting, September 7-11, 2008.

[6] Byoung-Uhn Bae, Specification of C2.2 Test, 1st PRG/MB Meeting of the OECD/NEA ATLAS Phase 3 Project, April 21-23, 2022.

[7] C.D. Fletcher, P.D. Bayless, C.B. Davis, M.G. Ortiz, S.M. Sloan, R.A. Shaw, R.R. Schultz, C.E. Slater, G.W. Johnsen, J.P. Adams, L.S. Ghan, D.E. Bessette, Adequacy Evaluation of RELAP5/MOD3, Version 3.2.1.2 for Simulating AP600 Small Break Loss-of-Coolant Accidents, INEL-96/0400, April 1997

[8] Byoung-Uhn Bae, Seok Cho, Kyoung-Ho Kang, Test Report on the OECD-ATLAS2 B3.2 Test: Direct Vessel Injection (DVI) Line Intermediate Break Loss-of-Coolant-Accident (IBLOCA) Test with ATLAS, OECD-ATLAS2-TR-19-02, KAERI, October 2019

[9] M. Ishii, I. Kataoka, Similarity Analysis and Scaling Criteria for LWRs Under Single Phase and Two-Phase Natural Circulation, NUREG/CR-3267, ANL-83-32, Argonne National Laboratory, 1983.

[10] Ki Yong Choi, Hyun Sik Park, Seok Cho, Kyoung Ho Kang, Nam Hyun Choi, Won Pil Baek, Yeon Sik Kim, Effects of Break Size on Direct Vessel Injection Line Break Accidents of the ATLAS, Nuclear Technology, Vol. 175, January 2011.

[11] Jae Bong Lee, Byoung-Uhn Bae, Yusun Park, Jongrok Kim, Yeon-Sik Kim, Seok Cho, Woojin Jeon, Hyun-Sik Park, Sung-Jae Yi, Sang-Ki Moon, Ki-Yong Choi, Chul-Hwa Song, Nam-Hyun Choi, Yong-cheol Shin, Kyoung-Ho Min, Kyoung-Ho Kang, Description Report of ATLAS Facility and Instrumentation (Second Revision), KAERI/TR-7218/2018, KAERI, 2018.

[12] Summary Report of the NEA ATLAS-2 Joint Project, NEA/CSNI/R(2021)6, OECD/NEA, February, 2022.

[13] Byoung-Uhn Bae, Jae-Bong Lee, Yu-Sun Park, Jong-Rok Kim, Seok Cho, Kyoung-Ho Kang, Integral Effect Test and MARS-KS Calculation with Uncertainty Propagation Analysis for Direct Vessel Injection Line Break Intermediate-Break Loss-of-Coolant Accident, Nuclear Technology, Vol. 207, p 680-691, October 2020.

[14] TRACE V5.0 Patch 7 User's Manual Volume 1: Input Specification, U.S. Nuclear Regulatory Commission, 2022.

[15] Kyung-Won Lee, Aeju Cheong, Andong Shin, Jae Soon Kim, Kyoung-Ho Kang, Assessment of Condensation Heat Transfer Models of TRACE V5.0 Patch 5 Using PASCAL Tests, NUREG/IA-0534, U.S. Nuclear Regulatory Commission, 2022.

[16] Kyung-Won Lee, Min Ki Cho, Andong Shin, Simulation of OECD/ATLAS A4.1 Test with TRACE Code, Transcations of the Korean Nuclear Society Virtual Spring Meeting, July 9-10, 2020.

[17] Steve M. Bajorect, Chris L. Hoxie, D. Scott Elkins, TRACE Pressurized Water Reactor Modeling Guidance, Revision 1, U.S. Nuclear Regulatory Commission, February 2015.

[18] TRACE V5.0 Patch 7 Theory Manual: Field Equations, Solution Method, and Physical Models, U.S. Nuclear Regulatory Commission, 2022.

NRC FORM 335
(12-2010)
NRCMD 3.7

U.S. NUCLEAR REGULATORY COMMISSION

BIBLIOGRAPHIC DATA SHEET

(See instructions on the reverse)

1. REPORT NUMBER
(Assigned by NRC, Add Vol., Supp., Rev., and Addendum Numbers, if any.)

NUREG/IA-0548

2. TITLE AND SUBTITLE

Assessment of TRACE V5.0 Patch 7 Using OECD-ATLAS2 B3.2 Test

3. DATE REPORT PUBLISHED

MONTH	YEAR
April	**2024**

4. FIN OR GRANT NUMBER

5. AUTHOR(S)

Seung Hun Yoo*, Kyung-Won Lee*, Dong Gu Kang*, Andong Shin*

6. TYPE OF REPORT

Technical

7. PERIOD COVERED (Inclusive Dates)

8. PERFORMING ORGANIZATION - NAME AND ADDRESS (If NRC, provide Division, Office or Region, U. S. Nuclear Regulatory Commission, and mailing address; if contractor, provide name and mailing address.)

*Korea Institute of Nuclear Safety (KINS)
62 Gwahak-ro, Yuseong-gu, Daejeon 34142, Republic of Korea

9. SPONSORING ORGANIZATION - NAME AND ADDRESS (If NRC, type "Same as above", if contractor, provide NRC Division, Office or Region, U. S. Nuclear Regulatory Commission, and mailing address.)

Division of Systems Analysis
Office of the Nuclear Regulatory Research
U.S. Nuclear Regulatory Commission
Washington, D.C. 20555-0001

10. SUPPLEMENTARY NOTES

K. Tien, Project Manager

11. ABSTRACT (200 words or less)

The assessment of TRACE V5.0 Patch 7 was performed using the OECD-ATLAS2 B3.2 test which is a 100% Direct Vessel Injection line break in the ATLAS referring to the APR1400. TRACE showed a generally good agreement with most of the sequence of events of the experiment including the injection timing of the Emergency Core Cooling System (ECCS), the minimum core level, and the occurrence of Loop Seal Clearing (LSC) but delayed in the core quenching time. The predicted integrated discharge flow, the mass flow rate of cold legs and hot legs, and the ECCS flow were well-matched with the experiment. TRACE predicted the same Maximum Cladding Temperature (MCT) at the same timing as the experiment. However, the predicted position of the MCT was different from the experiment due to the different predicted local behaviors and the predicted core quenching time was delayed. Through sensitivity studies, it was found that the cladding temperature generally increased in proportion to the break size and the most decisive factor in determining the cladding temperature is the behavior of the minimum core level. In conclusion, TRACE showed an excellent capability to predict the same MCT at the same timing as the experiment. However, it showed a reasonable capability to predict the pressure drop in the reactor vessel for the region of the steam-dominant two-phase flow, the recovery of the core level, and the core quenching time.

12. KEY WORDS/DESCRIPTORS (List words or phrases that will assist researchers in locating the report.)

APR1400, OECD-ATLAS2 B3.2, DVI Line Break, IBLOCA, MLOCA, Loop Seal Clearing, TRACE V5.0 Patch 7

13. AVAILABILITY STATEMENT

unlimited

14. SECURITY CLASSIFICATION

(This Page)
unclassified

(This Report)
unclassified

15. NUMBER OF PAGES

16. PRICE

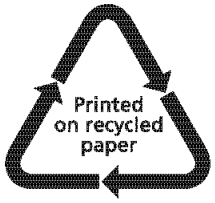

Federal Recycling Program

UNITED STATES
NUCLEAR REGULATORY COMMISSION
WASHINGTON, DC 20555-0001

OFFICIAL BUSINESS